

On the full quantum trispectrum in multi-field DBI inflation

Shuntaro Mizuno*[‡], Frederico Arroja[†][‡], and Kazuya Koyama[‡][‡]

[‡]*School of Physics and Astronomy, University of Nottingham, University Park, Nottingham NG7 2RD, UK; Research Center for the Early Universe (RESCEU), Graduate School of Science, The University of Tokyo, Tokyo 113-0033, Japan.*

[‡]*Yukawa Institute for Theoretical Physics, Kyoto University, Kyoto 606-8502, Japan.*

[‡]*Institute of Cosmology and Gravitation, University of Portsmouth, Portsmouth PO1 3FX, UK.*

(Dated: June 19, 2018)

We compute the leading order connected four-point function of the primordial curvature perturbation coming from the four-point function of the fields in multi-field DBI inflation models. We confirm that the consistency relations in the squeezed limit and in the counter-collinear limit hold as in single field models thanks to special properties of the DBI action. We also study the momentum dependence of the trispectra coming from the adiabatic, mixed and purely entropic contributions separately and we find that they have different momentum dependence. This means that if the amount of the transfer from the entropy perturbations to the curvature perturbation is significantly large, the trispectrum can distinguish multi-field DBI inflation models from single field DBI inflation models. A large amount of transfer $T_{\mathcal{R}S} \gg 1$ suppresses the tensor to scalar ratio $r \propto T_{\mathcal{R}S}^{-2}$ and the amplitude of the bispectrum $f_{NL}^{equi} \propto T_{\mathcal{R}S}^{-2}$ and so it can ease the severe observational constraints on the DBI inflation model based on string theory. On the other hand, it enhances the amplitude of the trispectrum $\tau_{NL}^{equi} \propto T_{\mathcal{R}S}^2 f_{NL}^{equi 2}$ for a given amplitude of the bispectrum.

I. INTRODUCTION

Precise measurements of the cosmic microwave background (CMB) anisotropies such as those obtained by the WMAP satellite [1] provide valuable information on the very early universe. Any theoretical model that attempts to explain the evolution of the universe before the big bang nucleosynthesis will also have to explain the observed CMB anisotropies. Even though these anisotropies are almost Gaussian, a small amount of non-Gaussianity is still allowed by the data [2, 3, 4] and future experiments such as PLANCK [5] might detect this small amount of the primordial non-Gaussianity. Even though the simplest slow-roll single field inflation models predict that the non-Gaussianity of the fluctuations should be very difficult to be detected [6], recently, theoretical models which can produce sizeable non-Gaussianity has been extensively studied by many authors [7, 8, 9, 10, 11, 12, 13, 14, 15, 16, 17, 18, 19, 20, 21, 22, 23, 24, 25, 26, 27, 28, 29, 30, 31, 32, 33, 34, 35, 36, 37, 38, 39, 40, 41, 42, 43, 44, 45, 46, 47, 48, 49, 50, 51, 52, 53, 54, 55, 56, 57, 58, 59, 60, 61, 62, 63, 64, 65, 66].

Among them, the Dirac-Born-Infeld (DBI) inflation model can produce large non-Gaussianity by the fact that the sound speed of the perturbations can be much smaller than one due to the non-trivial form of the kinetic term [67, 68]. DBI inflation models are also well motivated by string theory [13, 27, 69, 70, 71, 72]. In this model, the inflaton fields are identified with the positions of a moving D3 brane in the six-dimensional internal space. The dynamics of the D3 brane is described by the DBI action. However, recently it has been pointed out that single field DBI inflation driven by a mobile D3 brane with large non-Gaussianity might contradict with the current WMAP data. For current and stringent observational constraints and consequences of DBI-inflation see [73, 74, 75, 76, 77, 78, 79, 80, 81, 82, 83].

One way to avoid these constraints is to consider multi-field DBI models [36]. Since the position of the brane in each compact direction is described by a scalar field, DBI inflation is naturally a multi-field inflationary model [84]. As first pointed out by [85], in multi-field inflation models, the curvature perturbation is modified on large scales due to the entropy perturbation. Even though there are some works considering multi-field inflationary models with non-canonical kinetic terms [45, 86, 87, 88], the consistent analysis for the entropy modes in the multi-field DBI inflation model has started only very recently [35, 36, 37].

In [35, 36, 37], the three-point functions in the small sound speed limit and at leading order in the slow-roll expansion were obtained and it was shown that in addition to the purely adiabatic three-point function, there exists a mixed component $\langle Q_\sigma(\mathbf{k}_1)Q_s(\mathbf{k}_2)Q_s(\mathbf{k}_3) \rangle$ where Q_σ and Q_s are the adiabatic and the entropy perturbations, respectively. Since the momentum dependence of the three-point function from the adiabatic modes was shown to be identical

* shuntaro.mizuno@nottingham.ac.uk

† arroja@yukawa.kyoto-u.ac.jp

‡ Kazuya.Koyama@port.ac.uk

with the mixed component, the shape of the bispectrum of the curvature perturbations remains the same as in the single-field case, while the amplitude is affected by the entropy perturbation.

Even though previous works on the non-Gaussianity in the multi-field DBI inflation model are mainly limited to the bispectrum, it is expected that the cosmic microwave background (CMB) trispectrum also provides strong constraints on early universe models. At the moment, the constraints are rather weak given by $|\tau_{NL}| < 10^8$ [89, 90], where τ_{NL} denotes the size of the trispectrum. However, PLANCK will tighten the constraints significantly reaching $|\tau_{NL}| \sim 560$ [91]. Although these estimations are obtained assuming local type non-Gaussianity, we expect similar constraints can be obtained for non-Gaussianity from DBI inflation. It is also worth noting that the analysis in the single field DBI inflation model shows that the trispectrum from the contact interaction diagram is enhanced in the small sound speed limit as $\tau_{NL} \sim 1/c_s^4$ [28]. Even though the contribution from the scalar exchange interaction was overlooked in this analysis, recently, it has been confirmed that the same scaling holds for the trispectrum from this interaction [62, 63]. As in the bispectrum case [92], the observational constraints depend on the shape of the wave vectors' configuration. Therefore, it is important to calculate the full shape dependence of the trispectrum in the multi-field DBI inflation model. For the details of the observations of the CMB trispectrum, see [93, 94, 95].

For this purpose, recently we have calculated the quantum trispectrum from the contact interaction and obtained the simple understanding of the origin of the interaction terms of the multi-field DBI inflation [64]. In this paper, as a natural continuation, we will calculate the scalar exchange trispectrum and obtain the complete theoretical prediction for the quantum trispectrum of multi-field DBI inflation. For a related work, where only the purely entropic component of the quantum scalar exchange trispectrum was calculated, see version three of [55].

The structure of this paper is as follows. In the next section, we shall introduce the model and some basic notation. In section III we summarise the results obtained in [64] for the contact interaction trispectrum. After calculating the scalar exchange trispectrum in section IV, the momentum dependence of the trispectra coming from the adiabatic, mixed, and purely entropic contributions are studied separately in section V. The observational constraints on the multi-field DBI inflation model are discussed in section VI. Section VII is devoted to the conclusions.

II. THE MODEL

In this section, we will introduce the multi-field Dirac-Born-Infeld (DBI) inflationary model. We will present the background evolution equations and define some basic notation.

The multi-field DBI inflation model is described by the following action [96]

$$S = \frac{1}{2} \int d^4x \sqrt{-g} \left[R + 2\tilde{P}(\tilde{X}, \phi^I) \right],$$

$$\tilde{P}(\tilde{X}, \phi^I) = -\frac{1}{f(\phi^I)} \left(\sqrt{1 - 2f(\phi^I)\tilde{X}} - 1 \right) - V(\phi^I), \quad (1)$$

where we have set $8\pi G = 1$, R is the Ricci scalar, ϕ^I are the scalar fields ($I = 1, 2, \dots, N_\phi$), $f(\phi^I)$ and $V(\phi^I)$ are functions of the scalar fields determined by string theory configurations and \tilde{X} is defined in terms of the determinant $\mathcal{D} \equiv \det(\delta_\nu^\mu + f G_{IJ} \partial^\mu \phi^I \partial_\nu \phi^J)$ as $\tilde{X} = (1 - \mathcal{D})/(2f)$. Here G_{IJ} is the metric in the field space. We assume that \tilde{P} is a well behaved function of ϕ^I and \tilde{X} . It is also shown that \tilde{X} is related to the kinetic term of the scalar fields as [36, 37]

$$\tilde{X} = G_{IJ} X^{IJ} - 2f X_I^{[I} X_J^{J]} + 4f^2 X_I^{[I} X_J^J X_K^{K]} - 8f^3 X_I^{[I} X_J^J X_K^K X_L^{L]}, \quad (2)$$

$$X^{IJ} \equiv -\frac{1}{2} g^{\mu\nu} \partial_\mu \phi^I \partial_\nu \phi^J, \quad X_I^J = G_{IK} X^{KJ}, \quad (3)$$

where the brackets denote antisymmetrization. It is worth noting that even though $\tilde{X} = X (= G_{IJ} X^{IJ})$ in the homogeneous background, this does not hold if we take into account the inhomogeneous components.

In the background, we are interested in flat, homogeneous and isotropic Friedman-Robertson-Walker (FRW) universes described by the line element

$$ds^2 = -dt^2 + a^2(t) \delta_{ij} dx^i dx^j, \quad (4)$$

where $a(t)$ is the scale factor. The Friedman equation and the continuity equation read

$$3H^2 = E_0, \quad (5)$$

$$\dot{E}_0 = -3H(E_0 + \tilde{P}_0), \quad (6)$$

where the Hubble rate is $H = \dot{a}/a$, a dot denotes derivative with respect to cosmic time t , E_0 is the total energy of the fields which is given by

$$E_0 = 2X_0^{IJ} \tilde{P}_{0,X^{IJ}} - \tilde{P}_0, \quad (7)$$

and the subscript 0 denotes that the quantity is evaluated in the background.

For this model the speed of propagation of scalar perturbations (“speed of sound”), c_s , is given by

$$c_s^2 \equiv \left(\frac{\tilde{P}_{,\tilde{X}}}{\tilde{P}_{,\tilde{X}} + 2\tilde{X}\tilde{P}_{,\tilde{X}\tilde{X}}} \right)_0. \quad (8)$$

Since we are interested in the inflationary background, we assume that the form of $f(\phi^I)$ and $V(\phi^I)$ are chosen so that inflation is realized at least for 60 e-foldings. In order to characterize this background, we define the slow variation parameters, analogues of the slow-roll parameters, as:

$$\epsilon = -\frac{\dot{H}}{H^2} = \frac{X_0}{H^2 c_s}, \quad \iota = \frac{\dot{c}_s}{c_s H}, \quad \chi = \frac{c_s}{c_s H}. \quad (9)$$

We should note that these slow variation parameters are more general than the usual slow-roll parameters and that the smallness of these parameters does not imply that the field is rolling slowly. We assume that the rate of change of the speed of sound is small (as described by χ) but c_s is otherwise free to change between zero and one.

We shall consider perturbations on this FRW background. We decompose the scalar field ϕ^I into the background value ϕ_0^I and perturbation Q^I in the flat gauge as,

$$\phi^I(x, t) = \phi_0^I(t) + Q^I(x, t). \quad (10)$$

Furthermore, as was done in [97], we decompose the perturbations into instantaneous adiabatic and entropy perturbations, where the adiabatic direction corresponds to the direction of the background fields’ evolution while the entropy directions are orthogonal to this. We introduce an orthogonal basis e_n^I , with $n = 1, 2, \dots, N_\phi$, in the field space so that the orthonormality condition are given by [35]

$$e_n^I e_{mI} = \frac{1}{c_s} \delta_{mn} - \frac{1 - c_s^2}{c_s} \delta_{m1} \delta_{n1}, \quad (11)$$

where the adiabatic basis is defined as

$$e_1^I = \sqrt{\frac{c_s}{2X_0}} \phi_0^I. \quad (12)$$

Notice that the length of the basis vector e_1^I is c_s and that of the other basis vectors is $1/c_s$. If we consider the two-field case ($I = 1, 2$), the field perturbations are decomposed into the adiabatic field Q_σ and the entropy field Q_s as

$$Q^I = Q_\sigma e_1^I + Q_s e_2^I. \quad (13)$$

Hereafter, for simplicity, we will concentrate on the two-field case although the extension to more fields is straightforward.

For the single field model, since the comoving curvature perturbation \mathcal{R} is given by

$$\mathcal{R} = \left(\frac{\sqrt{c_s} H}{\sqrt{2X_0}} \right)_* Q_{\sigma*}, \quad (14)$$

the power spectrum of the primordial quantum fluctuation was given by [68]

$$\mathcal{P}_{\mathcal{R}_*}(k) = \frac{1}{36\pi^2} \frac{E_0^2}{E_0 + \tilde{P}_0} = \frac{1}{8\pi^2} \frac{H^2}{c_s \epsilon}, \quad (15)$$

where it should be evaluated at the time of horizon crossing $c_{s*} k = a_* H_*$. The spectral index is

$$n_{\mathcal{R}_*} - 1 = \frac{d \ln \mathcal{P}_{\mathcal{R}_*}(k)}{d \ln k} = -2\epsilon - \iota - \chi. \quad (16)$$

However, as explained in the following sections, this will not be the case for multi-field models.

III. THE TRISPECTRUM FROM THE CONTACT INTERACTION

In this and next sections, we will derive the four-point functions of the field perturbations at leading order in the slow-roll expansion and in the small sound speed limit. There are two important tree-level diagrams for the trispectrum. One is a diagram where the interaction occurs at a point, i.e. a contact interaction diagram and the other is a diagram where a scalar mode is exchanged. In the single field DBI inflation model, it was recently shown by [62, 63] that both contributions are comparable. Because it is expected that this is also true for the two-field DBI inflation model, it is necessary to consider both contributions. In this section, we summarize the calculation of the four-point functions of the field perturbations at horizon crossing coming from the contact interaction diagram [64]. In the next section, we shall calculate the scalar exchange four-point function.

Using the approximations mentioned above and following the ADM formalism [6, 17, 18, 98], the action up to fourth order can be calculated as [64]

$$S_{(2)}^{(main)} = \frac{1}{2} \int dt d^3x \frac{a^3}{c_s^2} \left[\dot{Q}_\sigma^2 + \dot{Q}_s^2 - \frac{c_s^2}{a^2} \left(\partial_i Q_\sigma \partial^i Q_\sigma + \partial_i Q_s \partial^i Q_s \right) \right], \quad (17)$$

$$S_{(3)}^{(main)} = \frac{1}{2} \int dt d^3x \frac{a^3}{\sqrt{2X_0 c_s^7}} \left[\dot{Q}_\sigma^3 + \dot{Q}_\sigma \dot{Q}_s^2 + \frac{c_s^2}{a^2} \left((\partial_i Q_s \partial^i Q_s - \partial_i Q_\sigma \partial^i Q_\sigma) \dot{Q}_\sigma - 2 (\partial_i Q_\sigma \partial^i Q_s) \dot{Q}_s \right) \right], \quad (18)$$

$$S_{(4)}^{(main)} = \frac{1}{16} \int dx^3 dt \frac{a^3}{c_s^5 X_0} \left[5 \dot{Q}_\sigma^4 + 6 \dot{Q}_\sigma^2 \dot{Q}_s^2 + \dot{Q}_s^4 - \frac{2c_s^2}{a^2} \left(3 \dot{Q}_\sigma^2 \partial_i Q_\sigma \partial^i Q_\sigma - \dot{Q}_\sigma^2 \partial_i Q_s \partial^i Q_s + 4 \dot{Q}_\sigma \dot{Q}_s \partial_i Q_\sigma \partial^i Q_s \right. \right. \\ \left. \left. + \dot{Q}_s^2 \partial_i Q_\sigma \partial^i Q_\sigma + \dot{Q}_s^2 \partial_i Q_s \partial^i Q_s \right) \right. \\ \left. + \frac{c_s^4}{a^4} \left((\partial_i Q_\sigma \partial^i Q_\sigma)^2 - 2 (\partial_i Q_\sigma \partial^i Q_\sigma) (\partial_j Q_s \partial^j Q_s) + 4 (\partial_i Q_\sigma \partial^i Q_s)^2 + (\partial_i Q_s \partial^i Q_s)^2 \right) \right]. \quad (19)$$

It is worth noting that Eqs. (17), (18) and (19) can also be derived using a simpler method based on a Lorentz boost from the frame where the brane is at rest to the frame where the brane is moving [64].

Based on these actions, we can obtain the third- and fourth-order interaction Hamiltonian densities as [64]

$$\mathcal{H}_{(3)}^{int} = \frac{-a^3}{2\sqrt{2X_0 c_s^7}} \left[\dot{Q}_\sigma^3 + \dot{Q}_\sigma \dot{Q}_s^2 - \frac{c_s^2}{a^2} \left\{ \dot{Q}_\sigma (\partial_i Q_\sigma \partial^i Q_\sigma - \partial_i Q_s \partial^i Q_s) + 2 \dot{Q}_s \partial_i Q_\sigma \partial^i Q_s \right\} \right], \quad (20)$$

$$\mathcal{H}_{(4)}^{int} = \frac{a^3}{4X_0 c_s^5} \left[\dot{Q}_\sigma^4 + \dot{Q}_\sigma^2 \dot{Q}_s^2 + \frac{c_s^2}{a^2} \left\{ (\partial_i Q_s \partial^i Q_s) \dot{Q}_\sigma^2 + (\partial_i Q_s \partial^i Q_s) \dot{Q}_s^2 \right\} \right], \quad (21)$$

where here, Q_σ and Q_s are the interaction picture fields. One important remark is that while the cubic part of \mathcal{H}^{int} is the opposite sign of the cubic Lagrangian density \mathcal{L}^{int} , this is generally not true at fourth order.

From the second-order action, we can solve for the perturbations and quantize them according to the standard procedures of quantum field theory:

$$Q_n(\eta, \mathbf{x}) = \frac{1}{(2\pi)^3} \int d^3\mathbf{k} \left[u_n(\eta, \mathbf{k}) a_n(\mathbf{k}) + u_n^*(\eta, -\mathbf{k}) a_n^\dagger(-\mathbf{k}) \right] e^{i\mathbf{k}\cdot\mathbf{x}}, \quad (22)$$

where $a_n(\mathbf{k})$ and $a_n^\dagger(-\mathbf{k})$ are the annihilation and creation operator respectively, which satisfy the usual commutation relations:

$$[a_n(\mathbf{k}_1), a_m^\dagger(\mathbf{k}_2)] = (2\pi)^3 \delta^{(3)}(\mathbf{k}_1 - \mathbf{k}_2) \delta_{nm}, \quad [a_n(\mathbf{k}_1), a_m(\mathbf{k}_2)] = [a_n^\dagger(\mathbf{k}_1), a_m^\dagger(\mathbf{k}_2)] = 0. \quad (23)$$

At leading order, solutions for the mode functions are given by

$$u_n(\eta, \mathbf{k}) = A_n \frac{1}{k^{3/2}} (1 + ikc_s \eta) e^{-ikc_s \eta}. \quad (24)$$

The two point correlation function is then obtained as

$$\langle 0 | Q_n(\eta = 0, \mathbf{k}_1) Q_m(\eta = 0, \mathbf{k}_2) | 0 \rangle = (2\pi)^3 \delta^{(3)}(\mathbf{k}_1 + \mathbf{k}_2) \mathcal{P}_{Q_n} \frac{2\pi^2}{k_1^3} \delta_{nm}, \quad (25)$$

where the power spectrum is defined as

$$\mathcal{P}_{Q_n} = \frac{|A_n|^2}{2\pi^2}, \quad |A_\sigma|^2 = |A_s|^2 = \frac{H^2}{2c_s} \equiv N^2, \quad (26)$$

and it should be evaluated at the time of the sound horizon crossing $c_{s*}k_1 = a_*H_*$.

In terms of these quantum operators, the connected four-point correlation function coming from the contact interaction diagram is given by [99]

$$\begin{aligned} \langle \Omega | Q_m(0, \mathbf{k}_1) Q_n(0, \mathbf{k}_2) Q_p(0, \mathbf{k}_3) Q_q(0, \mathbf{k}_4) | \Omega \rangle^{CI} = \\ -i \int_{-\infty}^0 d\eta \langle 0 | \left[Q_m(0, \mathbf{k}_1) Q_n(0, \mathbf{k}_2) Q_p(0, \mathbf{k}_3) Q_q(0, \mathbf{k}_4), H_{(4)}^{int}(\eta) \right] | 0 \rangle, \end{aligned} \quad (27)$$

where Q_m on the r.h.s. of the equation are the interaction picture fields and $H_{(4)}^{int}$ is the integral of the fourth-order Hamiltonian density (21), that is, $H_{(4)}^{int} = \int d^3x \mathcal{H}_{(4)}^{int}$.

The purely adiabatic, purely entropic and mixed components are respectively given by

$$\langle \Omega | Q_\sigma(0, \mathbf{k}_1) Q_\sigma(0, \mathbf{k}_2) Q_\sigma(0, \mathbf{k}_3) Q_\sigma(0, \mathbf{k}_4) | \Omega \rangle^{CI} = (2\pi)^3 \delta^{(3)} \left(\sum_{i=1}^4 \mathbf{k}_i \right) \frac{H^8}{2X_0 c_s^6} \frac{1}{\prod_{i=1}^4 k_i^3} (-36A_1), \quad (28)$$

$$A_1 = \frac{\prod_{i=1}^4 k_i^2}{K^5}, \quad K = \sum_{i=1}^4 k_i, \quad (29)$$

$$\langle \Omega | Q_s(0, \mathbf{k}_1) Q_s(0, \mathbf{k}_2) Q_s(0, \mathbf{k}_3) Q_s(0, \mathbf{k}_4) | \Omega \rangle^{CI} = (2\pi)^3 \delta^{(3)} \left(\sum_{i=1}^4 \mathbf{k}_i \right) \frac{H^8}{2X_0 c_s^6} \frac{1}{\prod_{i=1}^4 k_i^3} \left(-\frac{1}{8} A_2 \right), \quad (30)$$

$$A_2 = \frac{k_1^2 k_2^2 (\mathbf{k}_3 \cdot \mathbf{k}_4)}{K^3} \left(1 + \frac{3(k_3 + k_4)}{K} + \frac{12k_3 k_4}{K^2} \right) + \text{perm.} \quad (31)$$

$$\langle \Omega | Q_\sigma(0, \mathbf{k}_1) Q_\sigma(0, \mathbf{k}_2) Q_s(0, \mathbf{k}_3) Q_s(0, \mathbf{k}_4) | \Omega \rangle^{CI} = (2\pi)^3 \delta^{(3)} \left(\sum_{i=1}^4 \mathbf{k}_i \right) \frac{H^8}{2X_0 c_s^6} \frac{-1}{\prod_{i=1}^4 k_i^3} \left(6A_1 + \frac{1}{2} A_3 \right), \quad (32)$$

$$A_3 = \frac{k_1^2 k_2^2 (\mathbf{k}_3 \cdot \mathbf{k}_4)}{K^3} \left(1 + \frac{3(k_3 + k_4)}{K} + \frac{12k_3 k_4}{K^2} \right), \quad (33)$$

where ‘‘perm’’ denotes twenty three permutations of $\{k_1, k_2, k_3, k_4\}$.

Following the analysis of [100], if we describe the conversion of the entropy perturbation into the curvature perturbation by a transfer coefficient $T_{\mathcal{R}S}$, the final comoving curvature perturbation \mathcal{R} is expressed in terms of the adiabatic and entropy field perturbations as

$$\mathcal{R} = \mathcal{A}_\sigma Q_{\sigma*} + \mathcal{A}_s Q_{s*}, \quad \mathcal{A}_\sigma = \left(\frac{\sqrt{c_s} H}{\sqrt{2X_0}} \right)_*, \quad \mathcal{A}_s = T_{\mathcal{R}S} \left(\frac{\sqrt{c_s} H}{\sqrt{2X_0}} \right)_*. \quad (34)$$

This implies that the final comoving curvature perturbation power spectrum is

$$\mathcal{P}_{\mathcal{R}} = (1 + T_{\mathcal{R}S}^2) \mathcal{P}_{\mathcal{R}*}, \quad (35)$$

where the horizon crossing power spectrum $\mathcal{P}_{\mathcal{R}*}$ was given by Eq. (15).

At leading order, the connected four-point function of \mathcal{R} coming from the contact interaction diagram is given by ¹

$$\begin{aligned} \langle \mathcal{R}(\mathbf{k}_1) \mathcal{R}(\mathbf{k}_2) \mathcal{R}(\mathbf{k}_3) \mathcal{R}(\mathbf{k}_4) \rangle^{CI} = & \mathcal{A}_\sigma^4 \langle Q_\sigma(\mathbf{k}_1) Q_\sigma(\mathbf{k}_2) Q_\sigma(\mathbf{k}_3) Q_\sigma(\mathbf{k}_4) \rangle^{CI} \\ & + \mathcal{A}_\sigma^2 \mathcal{A}_s^2 \langle (Q_\sigma(\mathbf{k}_1) Q_\sigma(\mathbf{k}_2) Q_s(\mathbf{k}_3) Q_s(\mathbf{k}_4)) \rangle^{CI} + 5 \text{ perm.} \\ & + \mathcal{A}_s^4 \langle Q_s(\mathbf{k}_1) Q_s(\mathbf{k}_2) Q_s(\mathbf{k}_3) Q_s(\mathbf{k}_4) \rangle^{CI}, \end{aligned} \quad (36)$$

¹ There are other contributions to the connected four-point function of \mathcal{R} , for example those coming from the five- and six-point functions of the scalar fields that can be expressed in terms of the power spectrum using Wick’s theorem. In this work, we ignore these contributions because we are only interested in the intrinsically quantum four-point function. These extra terms are generated by the non-linear evolution outside the horizon and can be important

where “5 perm.” denotes five permutations of the four-momenta. Using Eqs. (28), (30) and (32), it is possible to show a simple relation among the three different terms in the previous equation, as

$$\langle Q_\sigma(\mathbf{k}_1)Q_\sigma(\mathbf{k}_2)Q_\sigma(\mathbf{k}_3)Q_\sigma(\mathbf{k}_4)\rangle^{CI} + \langle Q_s(\mathbf{k}_1)Q_s(\mathbf{k}_2)Q_s(\mathbf{k}_3)Q_s(\mathbf{k}_4)\rangle^{CI} = \langle Q_\sigma(\mathbf{k}_1)Q_\sigma(\mathbf{k}_2)Q_s(\mathbf{k}_3)Q_s(\mathbf{k}_4)\rangle^{CI} + 5 \text{ perm.} \quad (37)$$

This relation is perhaps less surprising if one notes that the different fourth-order interactions present in Eq. (21) also obey a similar relation, i.e. the purely adiabatic plus the purely entropic interactions (vertices) are equal to the mixed vertices.

Using the previous results, the contact interaction four-point function of \mathcal{R} can be written as

$$\begin{aligned} \langle \mathcal{R}(\mathbf{k}_1)\mathcal{R}(\mathbf{k}_2)\mathcal{R}(\mathbf{k}_3)\mathcal{R}(\mathbf{k}_4)\rangle^{CI} &= \mathcal{A}_\sigma^4 (1 + T_{\mathcal{RS}}^2) \left(\langle Q_\sigma(\mathbf{k}_1)Q_\sigma(\mathbf{k}_2)Q_\sigma(\mathbf{k}_3)Q_\sigma(\mathbf{k}_4)\rangle^{CI} \right. \\ &\quad \left. + T_{\mathcal{RS}}^2 \langle Q_s(\mathbf{k}_1)Q_s(\mathbf{k}_2)Q_s(\mathbf{k}_3)Q_s(\mathbf{k}_4)\rangle^{CI} \right). \end{aligned} \quad (38)$$

One immediately sees that if the transfer coefficient is non-zero, one can in principle use the trispectrum to distinguish single field from multi-field DBI inflation.

IV. THE TRISPECTRUM FROM THE SCALAR EXCHANGE INTERACTION

In this section, we will calculate the four-point functions of the field perturbations at horizon crossing coming from a diagram where a scalar mode is exchanged. Within the “interaction picture” formalism [99], to calculate the four-point function resulting from a correlation established via the exchange of a scalar mode, one needs to evaluate the following time integrals

$$\begin{aligned} &\langle \Omega | Q_m(0, \mathbf{k}_1) Q_n(0, \mathbf{k}_2) Q_p(0, \mathbf{k}_3) Q_q(0, \mathbf{k}_4) | \Omega \rangle^{SE} \\ &= - \int_{-\infty}^0 d\eta \int_{-\infty}^{\eta} d\tilde{\eta} \langle 0 | \left[\left[Q_m(0, \mathbf{k}_1) Q_n(0, \mathbf{k}_2) Q_p(0, \mathbf{k}_3) Q_q(0, \mathbf{k}_4), H_{(3)}^{int}(\eta) \right], H_{(3)}^{int}(\tilde{\eta}) \right] | 0 \rangle, \end{aligned} \quad (39)$$

where Q_m on the r.h.s. of the equation are the interaction picture fields and $H_{(3)}^{int}$ is the integral of the third-order Hamiltonian density (20), that is, $H_{(3)}^{int} = \int d^3x \mathcal{H}_{(3)}^{int}$.

The calculation of these time integrals is rather long and tedious. In Appendix A, we present an elegant and simple way of evaluating these contributions. This method is based on diagrams and simple rules that make the origin and physical meaning of all the different terms in the following expressions very clear. The purely adiabatic four-point

function coming from the scalar exchange diagrams is identical to the single field one [62], and it is given by

$$\begin{aligned}
\langle \Omega | Q_\sigma(0, \mathbf{k}_1) Q_\sigma(0, \mathbf{k}_2) Q_\sigma(0, \mathbf{k}_3) Q_\sigma(0, \mathbf{k}_4) | \Omega \rangle^{SE} &= (2\pi)^3 \delta^{(3)}(\mathbf{K}) \frac{H^4}{16 X_0 c_s^9 (k_1 k_2 k_3 k_4)^{\frac{3}{2}}} \times \\
&\left[-9 \left(\mathcal{F}_1(k_1, k_2, -k_{12}, k_3, k_4, k_{12}) - \mathcal{F}_1(-k_1, -k_2, -k_{12}, k_3, k_4, k_{12}) \right) \right. \\
&- 3c_s^2 \left((\mathbf{k}_3 \cdot \mathbf{k}_4) \left(\mathcal{F}_3(k_1, k_2, -k_{12}, k_{12}, k_3, k_4) - \mathcal{F}_3(-k_1, -k_2, -k_{12}, k_{12}, k_3, k_4) \right) \right. \\
&\quad - 2(\mathbf{k}_{34} \cdot \mathbf{k}_4) \left(\mathcal{F}_3(k_1, k_2, -k_{12}, k_3, k_4, k_{12}) - \mathcal{F}_3(-k_1, -k_2, -k_{12}, k_3, k_4, k_{12}) \right) \\
&\quad + (\mathbf{k}_1 \cdot \mathbf{k}_2) \left(\mathcal{F}_4(-k_{12}, k_1, k_2, k_3, k_4, k_{12}) - \mathcal{F}_4(-k_{12}, -k_1, -k_2, k_3, k_4, k_{12}) \right) \\
&\quad \left. \left. - 2(\mathbf{k}_{12} \cdot \mathbf{k}_2) \left(\mathcal{F}_4(k_1, k_2, -k_{12}, k_3, k_4, k_{12}) - \mathcal{F}_4(-k_1, -k_2, -k_{12}, k_3, k_4, k_{12}) \right) \right) \right) \\
&- c_s^4 \left((\mathbf{k}_1 \cdot \mathbf{k}_2)(\mathbf{k}_3 \cdot \mathbf{k}_4) \left(\mathcal{F}_2(-k_{12}, k_1, k_2, k_{12}, k_3, k_4) - \mathcal{F}_2(-k_{12}, -k_1, -k_2, k_{12}, k_3, k_4) \right) \right. \\
&\quad - 2(\mathbf{k}_1 \cdot \mathbf{k}_2)(\mathbf{k}_{34} \cdot \mathbf{k}_4) \left(\mathcal{F}_2(-k_{12}, k_1, k_2, k_3, k_4, k_{12}) - \mathcal{F}_2(-k_{12}, -k_1, -k_2, k_3, k_4, k_{12}) \right) \\
&\quad - 2(\mathbf{k}_{12} \cdot \mathbf{k}_2)(\mathbf{k}_3 \cdot \mathbf{k}_4) \left(\mathcal{F}_2(k_1, k_2, -k_{12}, k_{12}, k_3, k_4) - \mathcal{F}_2(-k_1, -k_2, -k_{12}, k_{12}, k_3, k_4) \right) \\
&\quad \left. \left. + 4(\mathbf{k}_{12} \cdot \mathbf{k}_2)(\mathbf{k}_{34} \cdot \mathbf{k}_4) \left(\mathcal{F}_2(k_1, k_2, -k_{12}, k_3, k_4, k_{12}) - \mathcal{F}_2(-k_1, -k_2, -k_{12}, k_3, k_4, k_{12}) \right) \right) \right) \right] \\
&+ 23 \text{ permutations of } \{k_1, k_2, k_3, k_4\}, \tag{40}
\end{aligned}$$

where $\mathbf{K} = \mathbf{k}_1 + \mathbf{k}_2 + \mathbf{k}_3 + \mathbf{k}_4$ and the information of the shape of the trispectrum is encoded in the \mathcal{F}_i functions defined by Eqs. (B1), (B2), (B3) and (B4) in Appendix B. In the previous expression, ‘‘permutations’’ denote the other twenty three terms that result from the permutations of $\{k_1, k_2, k_3, k_4\}$ in the preceding term.

The mixed component of the four-point function coming from the scalar exchange diagrams is

$$\begin{aligned}
\langle \Omega | Q_\sigma(0, \mathbf{k}_1) Q_\sigma(0, \mathbf{k}_2) Q_s(0, \mathbf{k}_3) Q_s(0, \mathbf{k}_4) | \Omega \rangle^{SE} + 5 \text{ terms} &= (2\pi)^3 \delta^{(3)}(\mathbf{K}) \frac{H^4}{16 X_0 c_s^9 (k_1 k_2 k_3 k_4)^{\frac{3}{2}}} \times \\
&\left[-10 \left(\mathcal{F}_1(k_1, k_2, -k_{12}, k_3, k_4, k_{12}) - \mathcal{F}_1(-k_1, -k_2, -k_{12}, k_3, k_4, k_{12}) \right) \right. \\
&+ 2c_s^2 \left(-(\mathbf{k}_3 \cdot \mathbf{k}_4) \left(\mathcal{F}_3(k_1, k_2, -k_{12}, k_{12}, k_3, k_4) - \mathcal{F}_3(-k_1, -k_2, -k_{12}, k_{12}, k_3, k_4) \right) \right. \\
&\quad + 4(\mathbf{k}_{34} \cdot \mathbf{k}_4) \left(\mathcal{F}_3(k_1, k_2, -k_{12}, k_3, k_4, k_{12}) - \mathcal{F}_3(-k_1, -k_2, -k_{12}, k_3, k_4, k_{12}) \right) \\
&\quad - (\mathbf{k}_1 \cdot \mathbf{k}_2) \left(\mathcal{F}_4(-k_{12}, k_1, k_2, k_3, k_4, k_{12}) - \mathcal{F}_4(-k_{12}, -k_1, -k_2, k_3, k_4, k_{12}) \right) \\
&\quad \left. \left. + 4(\mathbf{k}_{12} \cdot \mathbf{k}_2) \left(\mathcal{F}_4(k_1, k_2, -k_{12}, k_3, k_4, k_{12}) - \mathcal{F}_4(-k_1, -k_2, -k_{12}, k_3, k_4, k_{12}) \right) \right) \right) \\
&- 2c_s^4 \left((\mathbf{k}_1 \cdot \mathbf{k}_2)(\mathbf{k}_3 \cdot \mathbf{k}_4) \left(\mathcal{F}_2(-k_{12}, k_1, k_2, k_{12}, k_3, k_4) - \mathcal{F}_2(-k_{12}, -k_1, -k_2, k_{12}, k_3, k_4) \right) \right. \\
&\quad + 4(\mathbf{k}_{12} \cdot \mathbf{k}_2)(\mathbf{k}_{34} \cdot \mathbf{k}_4) \left(\mathcal{F}_2(k_1, k_2, -k_{12}, k_3, k_4, k_{12}) - \mathcal{F}_2(-k_1, -k_2, -k_{12}, k_3, k_4, k_{12}) \right) \left. \right) \right] \\
&+ 23 \text{ permutations of } \{k_1, k_2, k_3, k_4\}. \tag{41}
\end{aligned}$$

Finally, the purely entropic four-point function coming from the scalar exchange diagrams is

$$\begin{aligned}
\langle \Omega | Q_s(0, \mathbf{k}_1) Q_s(0, \mathbf{k}_2) Q_s(0, \mathbf{k}_3) Q_s(0, \mathbf{k}_4) | \Omega \rangle^{SE} &= (2\pi)^3 \delta^{(3)}(\mathbf{K}) \frac{H^4}{16 X_0 c_s^9 (k_1 k_2 k_3 k_4)^{\frac{3}{2}}} \times \\
&\left[- \left(\mathcal{F}_1(k_1, k_2, -k_{12}, k_3, k_4, k_{12}) - \mathcal{F}_1(-k_1, -k_2, -k_{12}, k_3, k_4, k_{12}) \right) \right. \\
&+ c_s^2 \left((\mathbf{k}_3 \cdot \mathbf{k}_4) \left(\mathcal{F}_3(k_1, k_2, -k_{12}, k_{12}, k_3, k_4) - \mathcal{F}_3(-k_1, -k_2, -k_{12}, k_{12}, k_3, k_4) \right) \right. \\
&\quad + 2(\mathbf{k}_{34} \cdot \mathbf{k}_4) \left(\mathcal{F}_3(k_1, k_2, -k_{12}, k_3, k_4, k_{12}) - \mathcal{F}_3(-k_1, -k_2, -k_{12}, k_3, k_4, k_{12}) \right) \\
&\quad + (\mathbf{k}_1 \cdot \mathbf{k}_2) \left(\mathcal{F}_4(-k_{12}, k_1, k_2, k_3, k_4, k_{12}) - \mathcal{F}_4(-k_{12}, -k_1, -k_2, k_3, k_4, k_{12}) \right) \\
&\quad \left. \left. + 2(\mathbf{k}_{12} \cdot \mathbf{k}_2) \left(\mathcal{F}_4(k_1, k_2, -k_{12}, k_3, k_4, k_{12}) - \mathcal{F}_4(-k_1, -k_2, -k_{12}, k_3, k_4, k_{12}) \right) \right) \right. \\
&- c_s^4 \left((\mathbf{k}_1 \cdot \mathbf{k}_2) (\mathbf{k}_3 \cdot \mathbf{k}_4) \left(\mathcal{F}_2(-k_{12}, k_1, k_2, k_{12}, k_3, k_4) - \mathcal{F}_2(-k_{12}, -k_1, -k_2, k_{12}, k_3, k_4) \right) \right. \\
&\quad + 2(\mathbf{k}_1 \cdot \mathbf{k}_2) (\mathbf{k}_{34} \cdot \mathbf{k}_4) \left(\mathcal{F}_2(-k_{12}, k_1, k_2, k_3, k_4, k_{12}) - \mathcal{F}_2(-k_{12}, -k_1, -k_2, k_3, k_4, k_{12}) \right) \\
&\quad + 2(\mathbf{k}_{12} \cdot \mathbf{k}_2) (\mathbf{k}_3 \cdot \mathbf{k}_4) \left(\mathcal{F}_2(k_1, k_2, -k_{12}, k_{12}, k_3, k_4) - \mathcal{F}_2(-k_1, -k_2, -k_{12}, k_{12}, k_3, k_4) \right) \\
&\quad \left. \left. + 4(\mathbf{k}_{12} \cdot \mathbf{k}_2) (\mathbf{k}_{34} \cdot \mathbf{k}_4) \left(\mathcal{F}_2(k_1, k_2, -k_{12}, k_3, k_4, k_{12}) - \mathcal{F}_2(-k_1, -k_2, -k_{12}, k_3, k_4, k_{12}) \right) \right) \right] \\
&+ 23 \text{ permutations of } \{k_1, k_2, k_3, k_4\}. \tag{42}
\end{aligned}$$

The remaining possible four-point functions, $\langle \Omega | Q_\sigma Q_\sigma Q_\sigma Q_s | \Omega \rangle^{SE}$ and $\langle \Omega | Q_\sigma Q_s Q_s Q_s | \Omega \rangle^{SE}$, are zero at leading order in the slow-roll expansion and in the small sound speed limit.

As in the previous section, the connected four-point function of the curvature perturbation \mathcal{R} is related with the four-point function of the field perturbation as ²

$$\begin{aligned}
\langle \Omega | \mathcal{R}(\mathbf{k}_1) \mathcal{R}(\mathbf{k}_2) \mathcal{R}(\mathbf{k}_3) \mathcal{R}(\mathbf{k}_4) | \Omega \rangle^{SE} &= \mathcal{A}_\sigma^4 \langle \Omega | Q_\sigma(\mathbf{k}_1) Q_\sigma(\mathbf{k}_2) Q_\sigma(\mathbf{k}_3) Q_\sigma(\mathbf{k}_4) | \Omega \rangle^{SE} \\
&+ \mathcal{A}_\sigma^2 \mathcal{A}_s^2 \left(\langle \Omega | Q_\sigma(\mathbf{k}_1) Q_\sigma(\mathbf{k}_2) Q_s(\mathbf{k}_3) Q_s(\mathbf{k}_4) | \Omega \rangle^{SE} + 5 \text{ perms} \right) \\
&+ \mathcal{A}_s^4 \langle \Omega | Q_s(\mathbf{k}_1) Q_s(\mathbf{k}_2) Q_s(\mathbf{k}_3) Q_s(\mathbf{k}_4) | \Omega \rangle^{SE}, \tag{43}
\end{aligned}$$

Again, as in the case of the contact interaction trispectra, the scalar exchange trispectra obey

$$\langle Q_\sigma(\mathbf{k}_1) Q_\sigma(\mathbf{k}_2) Q_\sigma(\mathbf{k}_3) Q_\sigma(\mathbf{k}_4) \rangle^{SE} + \langle Q_s(\mathbf{k}_1) Q_s(\mathbf{k}_2) Q_s(\mathbf{k}_3) Q_s(\mathbf{k}_4) \rangle^{SE} = \langle Q_\sigma(\mathbf{k}_1) Q_\sigma(\mathbf{k}_2) Q_s(\mathbf{k}_3) Q_s(\mathbf{k}_4) \rangle^{SE} + 5 \text{ perm.} \tag{44}$$

Using this fact Eq. (43) can be simplified to

$$\begin{aligned}
\langle \mathcal{R}(\mathbf{k}_1) \mathcal{R}(\mathbf{k}_2) \mathcal{R}(\mathbf{k}_3) \mathcal{R}(\mathbf{k}_4) \rangle^{SE} &= \mathcal{A}_\sigma^4 (1 + T_{\mathcal{R}S}^2) \left(\langle Q_\sigma(\mathbf{k}_1) Q_\sigma(\mathbf{k}_2) Q_\sigma(\mathbf{k}_3) Q_\sigma(\mathbf{k}_4) \rangle^{SE} \right. \\
&\quad \left. + T_{\mathcal{R}S}^2 \langle Q_s(\mathbf{k}_1) Q_s(\mathbf{k}_2) Q_s(\mathbf{k}_3) Q_s(\mathbf{k}_4) \rangle^{SE} \right). \tag{45}
\end{aligned}$$

Finally, the total four-point function of \mathcal{R} , coming from the quantum four-point functions of the fields, is the sum

² Where again we ignore terms that can be expressed by copies of the power spectrum by using Wick's theorem.

of the contact interaction and scalar exchange contributions as

$$\begin{aligned} \langle \mathcal{R}(\mathbf{k}_1)\mathcal{R}(\mathbf{k}_2)\mathcal{R}(\mathbf{k}_3)\mathcal{R}(\mathbf{k}_4) \rangle^{total} &= \langle \mathcal{R}(\mathbf{k}_1)\mathcal{R}(\mathbf{k}_2)\mathcal{R}(\mathbf{k}_3)\mathcal{R}(\mathbf{k}_4) \rangle^{CI} + \langle \mathcal{R}(\mathbf{k}_1)\mathcal{R}(\mathbf{k}_2)\mathcal{R}(\mathbf{k}_3)\mathcal{R}(\mathbf{k}_4) \rangle^{SE} \\ &= \mathcal{A}_\sigma^4 (1 + T_{\mathcal{R}S}^2) \left[\langle Q_\sigma(\mathbf{k}_1)Q_\sigma(\mathbf{k}_2)Q_\sigma(\mathbf{k}_3)Q_\sigma(\mathbf{k}_4) \rangle^{CI} + \langle Q_\sigma(\mathbf{k}_1)Q_\sigma(\mathbf{k}_2)Q_\sigma(\mathbf{k}_3)Q_\sigma(\mathbf{k}_4) \rangle^{SE} \right. \\ &\quad \left. + T_{\mathcal{R}S}^2 \left(\langle Q_s(\mathbf{k}_1)Q_s(\mathbf{k}_2)Q_s(\mathbf{k}_3)Q_s(\mathbf{k}_4) \rangle^{CI} + \langle Q_s(\mathbf{k}_1)Q_s(\mathbf{k}_2)Q_s(\mathbf{k}_3)Q_s(\mathbf{k}_4) \rangle^{SE} \right) \right], \end{aligned} \quad (46)$$

where the different terms can be found in Eqs. (28), (40), (30) and (42). This constitutes one of the main results of this work.

From Eq. (46) we can read the exact momentum dependence of the trispectrum which is related with the four-point function as

$$\langle \mathcal{R}(\mathbf{k}_1)\mathcal{R}(\mathbf{k}_2)\mathcal{R}(\mathbf{k}_3)\mathcal{R}(\mathbf{k}_4) \rangle^{total} = (2\pi)^3 \delta^{(3)}(\mathbf{K}) T_{\mathcal{R}}(\mathbf{k}_1, \mathbf{k}_2, \mathbf{k}_3, \mathbf{k}_4). \quad (47)$$

In the next section we shall study the shape of the trispectrum in more detail.

V. THE SHAPE OF THE TRISPECTRUM AND THE NON-LINEARITY PARAMETER τ_{NL}

In this section, we will study the shape dependence of the different trispectra calculated in the previous sections. We will consider the so-called equilateral configuration. In the next subsection, we shall discuss some consistency relations that apply for the multi-field DBI trispectrum. After that, we will compute the non-linearity parameter τ_{NL} and we shall plot the different contributions (pure adiabatic and pure entropy) to the total τ_{NL} both in the equilateral case and in a non-equilateral configuration. It is worth noting that from Eqs. (37) and (44), the contribution from the mixed component can be given from the other two contributions.

A. Consistency relations

Here, we discuss whether the consistency relations obtained in the single field DBI inflation model can hold also for the multi-field DBI inflation model. In the following, as in [62], we will define the non-linearity parameter, which naively parameterizes the size of the trispectrum as

$$\begin{aligned} \tau_{NL}(\mathbf{k}_1, \mathbf{k}_2, \mathbf{k}_3, \mathbf{k}_4) &= \left(\frac{4\epsilon c_s}{H^2(1 + T_{\mathcal{R}S}^2)} \right)^3 T_{\mathcal{R}}(\mathbf{k}_1, \mathbf{k}_2, \mathbf{k}_3, \mathbf{k}_4) \prod_{i=1}^4 k_i^3 \\ &\quad \times \left[(k_1^3 k_2^3 + k_3^3 k_4^3) (k_{13}^{-3} + k_{14}^{-3}) + (k_1^3 k_4^3 + k_2^3 k_3^3) (k_{12}^{-3} + k_{13}^{-3}) + (k_1^3 k_3^3 + k_2^3 k_4^3) (k_{12}^{-3} + k_{14}^{-3}) \right]^{-1}, \end{aligned} \quad (48)$$

and we discuss behaviours of τ_{NL} .

First, we discuss the consistency relation in the squeezed limit. As first pointed out by Maldacena [6] and Seery *et al.* [31], all higher order correlators of \mathcal{R} in single field inflation obey consistency relations when one of the momentum vector is very small. Let us consider the limit $\mathbf{k}_1 \rightarrow 0$, which implies that the corresponding mode $\mathcal{R}(\mathbf{k}_1)$ leaves the horizon well before all other modes leave the horizon. By the time the remaining modes exit the horizon, $\mathcal{R}(\mathbf{k}_1)$ will be frozen as a super-horizon mode and its only effect is to deform the background if the mode with \mathbf{k}_1 which leaves the horizon earlier than the others is the adiabatic mode (σ). Then in this case, the trispectrum can be expressed as [31]

$$\langle \mathcal{R}(\mathbf{k}_1)\mathcal{R}(\mathbf{k}_2)\mathcal{R}(\mathbf{k}_3)\mathcal{R}(\mathbf{k}_4) \rangle \rightarrow -\tilde{\mathcal{P}}_{\mathcal{R}}(k_1) \frac{d}{H dt} \langle \mathcal{R}(\mathbf{k}_2)\mathcal{R}(\mathbf{k}_3)\mathcal{R}(\mathbf{k}_4) \rangle, \quad (49)$$

where the power spectrum $\tilde{\mathcal{P}}_{\mathcal{R}}(k)$ is given by $\langle \mathcal{R}(\mathbf{k}_1)\mathcal{R}(\mathbf{k}_2) \rangle = (2\pi)^3 \delta^{(3)}(\mathbf{k}_1 + \mathbf{k}_2) \tilde{\mathcal{P}}_{\mathcal{R}}(k_1)$. Using the fact that the bispectrum is $B_\zeta \propto c_s^{-2} \tilde{\mathcal{P}}_{\mathcal{R}}^2$, it follows that in the squeezed limit the trispectrum is $\mathcal{T}_R \propto (\epsilon c_s^{-2} \tilde{\mathcal{P}}_{\mathcal{R}}^3)$. Using $\tilde{\mathcal{P}}_{\mathcal{R}} \propto (c_s \epsilon)^{-1}$, one finds that the total non-linearity parameter τ_{NL} should be at most of order ϵc_s^{-2} (i.e. under our approximation it should vanish) when any of the momentum vectors goes to zero. From Eqs. (28), (30), (32), (40), (41) and (42), we can show that τ_{NL} scales as $\mathcal{O}(k_1^2)$, which means the consistency relation in the squeezed limit holds for the trispectrum in multi-field DBI inflation models.

However, if the mode with \mathbf{k}_1 is the entropy mode (s), this explanation can not be applied. Instead, the fact that at leading order in slow-roll, the third-order action is written as Eq. (18) and there are no three point functions like (sss) and ($s\sigma\sigma$) turns out to be crucial. Actually, if one of the entropy modes leaves the horizon and becomes classical, the combination of the remaining three variables are (sss) for pure entropy component and ($s\sigma\sigma$) for mixed component, respectively. As mentioned above, since these three-point correlations are absent at leading order in slow roll, the trispectrum vanishes in this limit.

Similarly, we can discuss the consistency relation in the counter-collinear limit for the trispectra coming from the scalar exchange diagram. According to [38], in the limit where the momentum of the scalar mode that is exchanged goes to zero, one can find a simple relation between the scalar exchange trispectrum and the power spectrum, in a similar way to Maldacena's consistency relations [6] (see also [28, 101, 102]) since one can treat this mode as a background again if this mode is an adiabatic mode. Let us suppose that the momentum of the exchanged adiabatic particle is k_{12} and that $k_{12} \ll k_1 \approx k_2, k_3 \approx k_4$. Then the mode associated with this scalar particle will cross the horizon much before the other k_i modes, where $i = 1, \dots, 4$, and it only rescale the spatial background where the k_i modes exist. Then, in the limit $\mathbf{k}_{12} \rightarrow 0$, the following relation should hold if the exchange mode is an adiabatic mode:

$$\langle \mathcal{R}(\mathbf{k}_1)\mathcal{R}(\mathbf{k}_2)\mathcal{R}(\mathbf{k}_3)\mathcal{R}(\mathbf{k}_4) \rangle^{SE} \rightarrow (2\pi)^3 \delta^{(3)}(\mathbf{K})(n_{\mathcal{R}} - 1)^2 \tilde{\mathcal{P}}_{\mathcal{R}}(k_{12})\tilde{\mathcal{P}}_{\mathcal{R}}(k_1)\tilde{\mathcal{P}}_{\mathcal{R}}(k_3). \quad (50)$$

The previous equation implies that in the counter-collinear limit, the scalar exchange non-linearity parameter τ_{NL}^{SE} is of order ϵ^2 (at leading order in our approximations this is equivalent to say that τ_{NL}^{SE} should vanish). From Eqs. (40), (41) and (42), the non-linearity parameter τ_{NL} is shown to scale as $\mathcal{O}(k_{12}^4)$. Therefore, the consistency relation in the counter-collinear limit holds for the trispectrum coming from the scalar exchange diagram generated from the multi-field DBI inflation model. For the trispectrum coming from the other diagram, since there is no k_{12} dependence, this consistency relation holds trivially.

For the pure adiabatic, pure entropy and part of the mixed component, the exchanged mode is always an adiabatic mode. Thus we can apply the above argument to show that τ_{NL} vanishes in this limit. On the other hand, if the mode with \mathbf{k}_{12} is the entropy mode, which happens for the mixed component, we cannot apply the above arguments. However, in this case, the four-point function becomes a square of the two-point function of ($s\sigma$). As was shown by Eq. (17), there is no two-point correlation between the adiabatic and entropy mode at leading order in slow-roll. This explains the consistency relation in the counter-collinear limit for the remaining part of the mixed component.

Now that we have checked the two important consistency relations, in the next subsection, we will concentrate on a concrete and best studied configuration in single field DBI inflation model, the so-called equilateral configuration [28, 31, 62, 63].

B. The shape of the trispectrum and τ_{NL} in the equilateral configuration

In this subsection, we shall study the shape of the trispectrum in the limit where all the four momentum vectors have the same magnitude k . If we denote the angle between \mathbf{k}_i and \mathbf{k}_j by θ_{ij} , then in this configuration, we have $\cos(\theta_{12}) = \cos(\theta_{34}) \equiv \cos(\theta_3)$, $\cos(\theta_{23}) = \cos(\theta_{14}) \equiv \cos(\theta_1)$, $\cos(\theta_{13}) = \cos(\theta_{24}) \equiv \cos(\theta_2)$ and $\cos(\theta_1) + \cos(\theta_2) + \cos(\theta_3) = -1$ due to momentum conservation. Contrary to what happens in the case of the bispectrum, the equilateral configuration conditions do not fix all degrees of freedom (dof) required to describe the shape of the trispectrum and we are left with two angular dof [31].

In the equilateral configuration, the contact interaction trispectrum is constant and only the scalar exchange trispectrum depends on the remaining angular dof, that we choose to be θ_1 and θ_2 . The plots of the shape of the scalar exchange trispectrum coming from the purely adiabatic component (the first term in Eq. (43)) and the purely entropy component (the last term in Eq. (43)) can be found in Fig. 1. Using Eq. (45), one can easily see that, for $T_{\mathcal{RS}} \ll 1$ the purely adiabatic component dominates while for $T_{\mathcal{RS}} \gg 1$, the purely entropy component dominates. Because the momentum dependence of the trispectrum changes depending on the value of $T_{\mathcal{RS}}$, the trispectrum can distinguish multi-field DBI inflation models from single field DBI inflation models if $T_{\mathcal{RS}}$ is significantly large. The exact analytical expressions for the different contributions in the scalar exchange trispectrum can be found in Appendix C.

Even though the trispectrum includes all the information, for practical purposes it is more convenient to use another quantity τ_{NL} defined in Eq. (48). In Fig. 2, we plot the non-linearity parameter τ_{NL}^{SE} for the purely adiabatic and purely entropy components calculated from the respective terms in the scalar exchange trispectrum, Eq. (43).

In Fig. 3, we plot the non-linearity parameter τ_{NL}^{CI} for the purely entropy component of the contact interaction trispectrum. The shape of the surfaces for the purely adiabatic and mixed components are the same as the one for the purely entropy component. However, the amplitudes are different, in particular, for the purely adiabatic plot, τ_{NL}^{CI} is negative. On the r.h.s. of Fig. 3, we plot the sum of the non-linearity parameters τ_{NL}^{CI} and τ_{NL}^{SE} that come

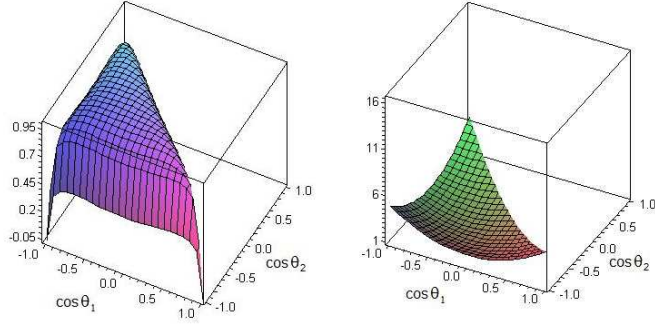


FIG. 1: The shape of the scalar exchange adiabatic (l.h.s panel) and pure entropy (r.h.s. panel) trispectra as functions of the variables $\cos \theta_1$ and $\cos \theta_2$. The amplitude of the trispectra at the point $\cos \theta_1 = \cos \theta_2 = -1/3$ has been normalized to unity.

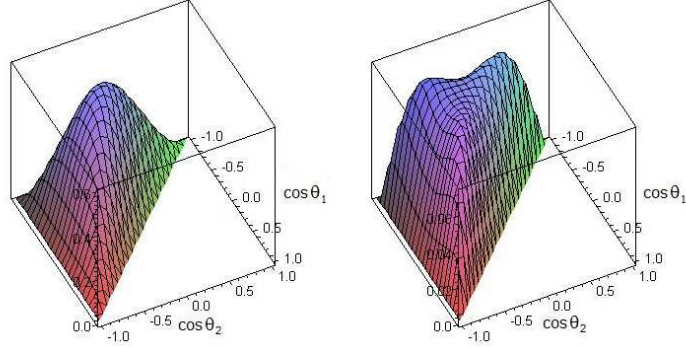


FIG. 2: Plots of the non-linearity parameter τ_{NL}^{SE} calculated from the scalar exchange adiabatic (l.h.s. panel) and pure entropy (r.h.s. panel) trispectra as functions of the variables $\cos \theta_1$ and $\cos \theta_2$. The amplitude of the first plot was rescaled by $c_s^4(1+T_{RS}^2)^3$, while the amplitude of the r.h.s. plot was rescaled by $c_s^4(1+T_{RS}^2)^3/T_{RS}^4$.

from purely entropic perturbations. If the transfer coefficient is large this will be the dominant shape in the total non-linearity parameter.

Notice that since the factor k_{ij}^3 is multiplying the trispectrum, in terms of τ_{NL} , we confirm the consistency relation in the counter-collinear limit of the trispectrum coming from pure adiabatic, mixed and pure entropy components. When $\cos \theta_1 = -1$ or $\cos \theta_2 = -1$ or $\cos \theta_3 = -1$ (on the diagonal lines in the plots of Fig. 2, when $\cos \theta_2 = -\cos \theta_1$) we can see the non-linearity parameters are zero.

In order to quote a number for the value of the non-linearity parameter, we need to fix the remaining two degrees of freedom (θ_1 and θ_2) and in this way fully specify the momentum vectors' configuration. In the single field DBI model, there are good reasons to believe that the maximum of τ_{NL} occurs for the equilateral configuration with $\cos(\theta_1) = \cos(\theta_2) = \cos(\theta_3) = -1/3$ [62]³. In the multi-field case, for some contributions (like for example, τ_{NL}^{SE} coming from the pure entropy trispectrum, as seen on the r.h.s. panel of Fig. 2) the non-linearity parameter is not maximized for this particular angular configuration. However, for the sake of comparison with the single field model, we shall obtain the non-linearity parameter in that configuration.

³ However, the definite proof that this is the case is still missing

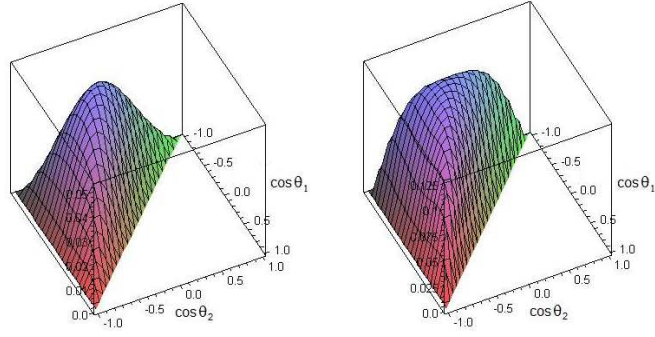


FIG. 3: L.h.s. panel: Plot of the non-linearity parameter τ_{NL}^{CI} calculated from the contact interaction pure entropy trispectrum as a function of $\cos\theta_1$ and $\cos\theta_2$. R.h.s. panel: Plot of the sum of τ_{NL}^{CI} and τ_{NL}^{SE} coming from the pure entropy trispectrum as a function of $\cos\theta_1$ and $\cos\theta_2$. The amplitude of the plots was rescaled by $c_s^4(1+T_{\mathcal{RS}}^2)^3/T_{\mathcal{RS}}^4$.

So, for the equilateral configuration, with $\cos(\theta_1) = \cos(\theta_2) = \cos(\theta_3) = -1/3$, we obtain

$$\tau_{NL4\sigma}^{CI} \sim -\frac{0.036}{c_s^4(1+T_{\mathcal{RS}}^2)^3}, \quad \tau_{NL\sigma\sigma ss}^{CI} \sim \frac{0.016T_{\mathcal{RS}}^2}{c_s^4(1+T_{\mathcal{RS}}^2)^3}, \quad \tau_{NL4s}^{CI} \sim \frac{0.052T_{\mathcal{RS}}^4}{c_s^4(1+T_{\mathcal{RS}}^2)^3}, \quad (51)$$

where the different values of τ_{NL} correspond to the three terms in the contact interaction trispectrum coming from the purely adiabatic, mixed and purely entropic components in Eq. (36), respectively.

Similarly, from the scalar exchange trispectrum we obtain

$$\tau_{NL4\sigma}^{SE} \sim \frac{0.60}{c_s^4(1+T_{\mathcal{RS}}^2)^3}, \quad \tau_{NL\sigma\sigma ss}^{SE} \sim \frac{0.67T_{\mathcal{RS}}^2}{c_s^4(1+T_{\mathcal{RS}}^2)^3}, \quad \tau_{NL4s}^{SE} \sim \frac{0.071T_{\mathcal{RS}}^4}{c_s^4(1+T_{\mathcal{RS}}^2)^3}, \quad (52)$$

where again the different values of τ_{NL} correspond to the three terms in the scalar exchange interaction trispectrum coming from the purely adiabatic, mixed and purely entropic components in Eq. (43), respectively.

It is worth mentioning that from Eqs. (37) and (44), both for the contact interaction (Eq. (51)) and the scalar exchange interaction (Eq. (52)), we can obtain the relation

$$\tau_{NL\sigma\sigma ss} = T_{\mathcal{RS}}^2 \tau_{NL4\sigma} + \frac{1}{T_{\mathcal{RS}}^2} \tau_{NL4s}. \quad (53)$$

Therefore, we conclude that the total non-linearity parameter τ_{NL} for the multi-field DBI inflation model in the equilateral configuration with equal angles between the momentum vectors is

$$\tau_{NL}^{tot\,equi} \sim \frac{0.56}{c_s^4(1+T_{\mathcal{RS}}^2)^3} + \frac{0.68T_{\mathcal{RS}}^2}{c_s^4(1+T_{\mathcal{RS}}^2)^3} + \frac{0.12T_{\mathcal{RS}}^4}{c_s^4(1+T_{\mathcal{RS}}^2)^3}. \quad (54)$$

It is worth noting that when there is no conversion of entropy perturbation into curvature perturbation, i.e. $T_{\mathcal{RS}} = 0$, Eq. (54) reproduces the result obtained in the single field DBI inflation model [62]. On the other hand, when the transfer coefficient is large, i.e. $T_{\mathcal{RS}} \gg 1$, the final curvature perturbation is mainly of entropy origin and the last term in Eq. (54) dominates over the others.

C. The non-linearity parameter τ_{NL} in a non-equilateral configuration

As we have mentioned before, the equilateral configuration is well investigated in the DBI inflation model. However, since there are five degrees of freedom to parameterize the shape of the trispectrum and the expression for the trispectrum is fairly complicated, non-equilateral configurations have attracted less attention. Because it has not been shown that the equilateral configuration maximizes the value of the non-linearity parameter, in this subsection we will consider a non-equilateral configuration.

In our previous work [62], we have studied the deviation from the equilateral configuration by fixing a particular set of degrees of freedom in the single field DBI inflation model case. Here, we apply the same approach and we study the behaviour of τ_{NL} in a non-equilateral configuration.

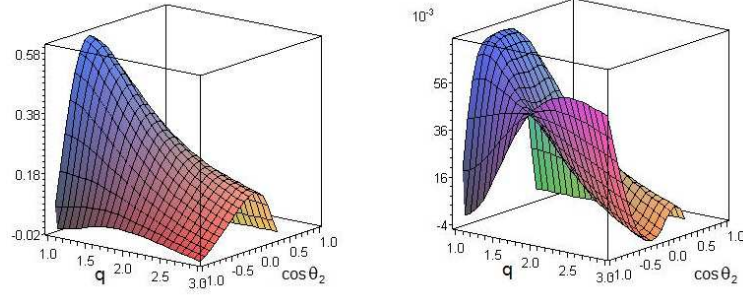


FIG. 4: Plots of the non-linearity parameter τ_{NL}^{SE} calculated from the scalar exchange adiabatic (l.h.s. panel) and pure entropy (r.h.s. panel) trispectra for non-equilateral configurations as functions of the momentum amplitude q and $\cos \theta_2$. The amplitude of the first plot was rescaled by $c_s^4(1+T_{\mathcal{RS}}^2)^3$, while the amplitude of the r.h.s. plot was rescaled by $c_s^4(1+T_{\mathcal{RS}}^2)^3/T_{\mathcal{RS}}^4$.

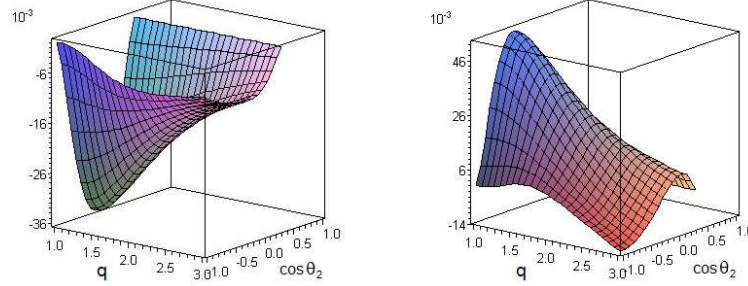


FIG. 5: Plots of the non-linearity parameter τ_{NL}^{CI} calculated from the contact interaction adiabatic (l.h.s. panel) and pure entropy (r.h.s. panel) trispectra for non-equilateral configurations as functions of the momentum amplitude q and $\cos \theta_2$. The amplitude of the first plot was rescaled by $c_s^4(1+T_{\mathcal{RS}}^2)^3$, while the amplitude of the r.h.s. plot was rescaled by $c_s^4(1+T_{\mathcal{RS}}^2)^3/T_{\mathcal{RS}}^4$.

We consider configurations where the two momentum vectors \mathbf{k}_3 and \mathbf{k}_4 have a different magnitude q from the magnitude of \mathbf{k}_1 and \mathbf{k}_2 that we normalized to unity. Then in this configuration, we have $\cos(\theta_{34}) \equiv \cos(\theta_3)$, $\cos(\theta_{23}) = \cos(\theta_{14}) \equiv \cos(\theta_1)$, $\cos(\theta_{13}) = \cos(\theta_{24}) \equiv \cos(\theta_2)$, $\cos(\theta_{12}) = q^2(1 + \cos(\theta_3)) - 1$. Momentum conservation implies $\cos \theta_3 = -(1/q)(\cos \theta_1 + \cos \theta_2) - 1$. We will allow one of the angular dof to vary freely, the other angular dof θ_1 is fixed by $\cos \theta_1 = -1/3$ to the value that gives us the maximum for the single field model. In Fig. 4, we plot the non-linearity parameter τ_{NL}^{SE} calculated from the scalar exchange adiabatic (l.h.s. panel) and entropic (r.h.s. panel) trispectra, respectively. The maximum appears at $q = 1$ and $\cos(\theta_2) = -1/3$, which supports the importance of the equilateral configuration. In Fig. 5, we plot the non-linearity parameter τ_{NL}^{CI} calculated from the contact interaction adiabatic (l.h.s. panel) and entropic (r.h.s. panel) trispectra, respectively. Comparing Figs. 4 and 5, one can see that around the maximum the purely adiabatic contribution coming from the contact interaction is smaller than the corresponding one coming from the scalar exchange interaction. Only for the entropy component, the amplitudes of the scalar exchange and contact interaction trispectra are comparable. We plot the sum of these two terms in Fig. 6. If the transfer coefficient is large this will be the dominant shape.

VI. OBSERVATIONAL CONSTRAINTS

Since we have obtained the full quantum trispectra for each component for the equilateral configuration with $\cos(\theta_1) = \cos(\theta_2) = \cos(\theta_3) = -1/3$, in terms of $T_{\mathcal{RS}}$, we are in a position to discuss the relation between $T_{\mathcal{RS}}$ and observable quantities. It was shown in [57] that in the small sound speed limit ($c_s^2 \ll 1$), the spectral index of the

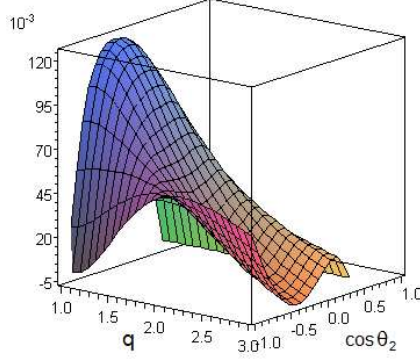


FIG. 6: Plot of the sum of the non-linearity parameters τ_{NL}^{SE} and τ_{NL}^{CI} calculated from the pure entropy trispectra, for non-equilateral configurations, as functions of the momentum amplitude q and $\cos\theta_2$. The amplitude of the plot was rescaled by $c_s^4(1 + T_{RS}^2)^3/T_{RS}^4$.

scalar perturbations $n_{\mathcal{R}}$ in two-field DBI inflation model can be written as

$$1 - n_{\mathcal{R}} \simeq \frac{\sqrt{3.1|f_{NL}^{equil}|}r}{4 \cos^3 \Theta} - \frac{\dot{f}}{Hf} + \alpha_* \sin(2\Theta) + 2\beta_* \sin^2 \Theta, \quad (55)$$

$$\text{with } \alpha = \frac{\xi}{aH}, \quad \beta = \frac{\chi}{2} - \frac{\iota}{2} - \frac{1}{3H^2} \left(\mu_s^2 + \frac{\xi^2}{a^2} \right), \quad \Theta = \arcsin \left(\frac{T_{RS}}{\sqrt{1 + T_{RS}^2}} \right), \quad (56)$$

where ι and χ are the slow-roll parameters defined in Eq. (9). ξ is the coupling between the adiabatic and entropy perturbation and μ_s is the mass of the entropy perturbation, which are model dependent quantities. In order to obtain Eq. (55), they used the following relations:

$$r = \frac{\mathcal{P}_T}{\mathcal{P}_{\mathcal{R}}} = 16\epsilon c_s \cos^2 \Theta, \quad (57)$$

$$f_{NL}^{equi} \simeq -\frac{1}{3.1c_s^2} \cos^2 \Theta, \quad (58)$$

where r is the tensor to scalar ratio and f_{NL}^{equi} parameterizes the size of the bispectrum in the equilateral configuration.

In the ultra-violet (UV) DBI model ($\dot{f} > 0$) and without entropy transfer, i.e. $T_{RS} = 0$ (or equivalently $\sin \Theta = 0$), Eq. (55) gives the well known stringent constraint as

$$r > \frac{4}{\sqrt{3.1|f_{NL}^{equi}|}} (1 - n_{\mathcal{R}}), \quad (59)$$

by which one obtains $r \geq 10^{-3}$ if one uses the observational constraints on f_{NL}^{equi} and $1 - n_{\mathcal{R}}$ from WMAP5 data [3]. On the other hand, since for general compact internal spaces, suggested by string theory, there is a geometrical constraint that limits r to be $r < 10^{-7}$ [77], the single field UV DBI inflation model is already excluded by the observational data.

However, if we take into account the transfer from the entropy perturbation, the last two terms in Eq. (55) are no longer negligible. Furthermore, from Eqs. (57) and (58), both r and f_{NL}^{equi} are suppressed by $\cos^2 \Theta$ which scales as $1/T_{RS}^2$ for $T_{RS} \gg 1$. Because of these factors, the constraint given by Eq. (59) cannot be applied and it is possible to satisfy the geometrical constraint $r < 10^{-7}$ if $T_{RS} \gg 1$ [57]. In such a case, since the last term of Eq. (54) will dominate over the other terms, τ_{NL}^{equi} can be expressed as $\tau_{NL}^{equi} \sim 1.14(f_{NL}^{equi})^2 T_{RS}^2$. Thus for a given f_{NL}^{equi} , τ_{NL}^{equi} is enhanced for a large transfer $T_{RS} \gg 1$, while the global magnitude of τ_{NL} is reduced, going like $1/T_{RS}^2$ in this case.

VII. CONCLUSIONS

In this work, we have obtained the full quantum trispectrum of the primordial curvature perturbation at leading order in the slow-roll expansion and in the small sound speed limit in multi-field DBI inflation models. Previously,

we had obtained the contact interaction trispectrum [64]. In this work we completed the calculation of the quantum trispectrum including the scalar exchange trispectrum.

We studied the momentum dependence of the trispectrum by separating it into the purely adiabatic, mixed and purely entropic components. For general configurations, as in the single field model, we confirmed that the consistency relations in the squeezed and in the counter-collinear limit hold. If a mode that crosses the horizon much before the other modes is an adiabatic one, these can be explained by the usual argument that the mode only changes the background (just like in the single field models). However, if the mode that crosses the horizon first is an entropic one, the consistency relations hold because of the absence of the two-point and three-point correlations among the modes remaining under the horizon scale. Essentially, the absence of these correlations is attributed to the particular properties of the DBI action discussed in [64].

In the equilateral configuration, we examined the momentum dependence of the scalar exchange trispectra as functions of the two remaining angular degrees of freedom. We found that the shape of the adiabatic, mixed, and purely entropic trispectra are different. This means that if the amount of the transfer from the entropy perturbation to the final curvature perturbation is significantly large, the trispectrum can distinguish multi-field DBI inflation models from single field DBI inflation models. In the equilateral configuration with $\cos\theta_1 = \cos\theta_2 = \cos\theta_3 = -1/3$, we showed that for the contributions for τ_{NL} coming from the adiabatic and mixed trispectra, the scalar exchange diagram is more important than the contact interaction diagram, while for the pure entropy contribution both diagrams are equally important. This suggests that for quantitative discussions, the analysis done in Ref. [55] taking into account only the scalar exchange diagram is insufficient, at least, in this configuration. We have also considered configurations where the equilateral conditions are not satisfied.

After obtaining the complete predictions for the quantum trispectrum in the multi-field DBI inflation model, we discussed the observational constraints on the non-linearity parameter, for the equilateral configuration mentioned above. In single field DBI inflation, some models based on string theory set-ups suffer from a severe constraint related with the geometrical structure of the compact internal spaces. However, in the presence of the transfer from the entropy mode, this constraint no longer holds. Furthermore, since both the tensor-to-scalar ratio and non-linearity parameter for the bispectrum are suppressed like $T_{\mathcal{RS}}^{-2}$ for a large transfer from the entropy mode to the curvature perturbation, it is easier to satisfy the corresponding constraints [57]. On the other hand, the trispectrum is enhanced like $\tau_{NL}^{equi} \propto T_{\mathcal{RS}}^2 f_{NL}^{equi\ 2}$ for a given amplitude of the bispectrum f_{NL}^{equi} , while the global magnitude of τ_{NL} is reduced, going like $1/T_{\mathcal{RS}}^2$ in this case.

In order to obtain a concrete value for the transfer coefficient $T_{\mathcal{RS}}$, we need a specific model. It would be interesting to study this mixing in specific string theory motivated models [103].

Note added: On the day this work appeared in the arXiv, the paper [104] was also submitted to the arXiv, it also calculates the trispectrum in multi-field DBI-inflation. While we have concentrated on the trispectrum coming from the intrinsically quantum four-point functions of the fields which are generated during inflation, Ref. [104], by assuming a specific model, showed that the contribution to the trispectrum coming from the super-horizon non-linear dynamics is also important.

Acknowledgments

We would like to thank Takahiro Tanaka for interesting discussions. SM and FA are supported by JSPS Research Fellowships. KK is supported by ERC, RCUK and STFC. SM is grateful to the ICG, Portsmouth for their hospitality when this work was completed.

APPENDIX A: THE DIAGRAMMATIC APPROACH TO THE TRISPECTRUM FROM THE SCALAR EXCHANGE INTERACTION

The calculation of the integrals in Eq. (39) is rather long and it is easy to forget some terms or permutations. In this appendix, we present a systematic and simple way to keep track of all the different contributions and permutations to the integrals in (39). This approach is based on diagrams and simple rules that allows one to read the respective contributions for the scalar exchange four-point function directly from the diagrams.

To calculate the scalar exchange four-point function we need to evaluate

$$\begin{aligned} & \langle \Omega | Q_m(0, \mathbf{k}_1) Q_n(0, \mathbf{k}_2) Q_p(0, \mathbf{k}_3) Q_q(0, \mathbf{k}_4) | \Omega \rangle^{SE} \\ & = - \int_{-\infty}^0 d\eta \int_{-\infty}^{\eta} d\tilde{\eta} \langle 0 | \left[\left[Q_m(0, \mathbf{k}_1) Q_n(0, \mathbf{k}_2) Q_p(0, \mathbf{k}_3) Q_q(0, \mathbf{k}_4), H_{(3)}^{int}(\eta) \right], H_{(3)}^{int}(\tilde{\eta}) \right] | 0 \rangle, \end{aligned} \quad (A1)$$

where on the l.h.s. of the equation Q_m are the interaction picture fields and $H_{(3)}^{int}$ is the third-order interaction Hamiltonian that can be found in Eq. (20) or

$$H_{(3)}^{int}(\eta) = H_1^{int}(\eta) + H_2^{int}(\eta) + H_3^{int}(\eta) + H_4^{int}(\eta) + H_5^{int}(\eta), \quad (\text{A2})$$

where the different type of interactions are

$$\begin{aligned} H_1^{int}(\eta) &\equiv \int d^3x g_1 a Q'_\sigma{}^3, & H_2^{int}(\eta) &\equiv \int d^3x g_2 a Q'_\sigma (\partial Q_\sigma)^2, & H_3^{int}(\eta) &\equiv \int d^3x g_3 a Q'_\sigma Q_s{}^2, \\ H_4^{int}(\eta) &\equiv \int d^3x g_4 a Q'_\sigma (\partial Q_s)^2, & H_5^{int}(\eta) &\equiv \int d^3x g_5 a Q'_s (\partial Q_\sigma) (\partial Q_s), \end{aligned} \quad (\text{A3})$$

where here Q_σ and Q_s are the interaction picture fields. The coupling constants are

$$g_1 = M, \quad g_2 = -c_s^2 M, \quad g_3 = M, \quad g_4 = c_s^2 M, \quad g_5 = -2c_s^2 M, \quad (\text{A4})$$

where $M = -\frac{1}{\sqrt{8X_0 c_s^2}}$. The integrand of Eq. (A1) can be written as

$$\begin{aligned} &\left[\left[Q_m(0, \mathbf{k}_1) Q_n(0, \mathbf{k}_2) Q_p(0, \mathbf{k}_3) Q_q(0, \mathbf{k}_4), H_{(3)}^{int}(\eta) \right], H_{(3)}^{int}(\tilde{\eta}) \right] \\ &= \sum_{i,j=1}^5 \left\{ F H_i^{int}(\eta) H_j^{int}(\tilde{\eta}) + H_j^{int}(\tilde{\eta}) H_i^{int}(\eta) F - H_j^{int}(\tilde{\eta}) F H_i^{int}(\eta) - H_i^{int}(\eta) F H_j^{int}(\tilde{\eta}) \right\} \end{aligned} \quad (\text{A5})$$

where we have defined F as $F \equiv Q_m(0, \mathbf{k}_1) Q_n(0, \mathbf{k}_2) Q_p(0, \mathbf{k}_3) Q_q(0, \mathbf{k}_4)$.

One can immediately see that at the leading order the only non-zero four-point functions are $\langle \Omega | Q_\sigma(0, \mathbf{k}_1) Q_\sigma(0, \mathbf{k}_2) Q_\sigma(0, \mathbf{k}_3) Q_\sigma(0, \mathbf{k}_4) | \Omega \rangle^{SE}$, $\langle \Omega | Q_s(0, \mathbf{k}_1) Q_s(0, \mathbf{k}_2) Q_\sigma(0, \mathbf{k}_3) Q_\sigma(0, \mathbf{k}_4) | \Omega \rangle^{SE}$ and $\langle \Omega | Q_s(0, \mathbf{k}_1) Q_s(0, \mathbf{k}_2) Q_s(0, \mathbf{k}_3) Q_s(0, \mathbf{k}_4) | \Omega \rangle^{SE}$. The four-point functions $\langle \Omega | Q_\sigma(0, \mathbf{k}_1) Q_\sigma(0, \mathbf{k}_2) Q_\sigma(0, \mathbf{k}_3) Q_s(0, \mathbf{k}_4) | \Omega \rangle^{SE}$ and $\langle \Omega | Q_\sigma(0, \mathbf{k}_1) Q_s(0, \mathbf{k}_2) Q_s(0, \mathbf{k}_3) Q_s(0, \mathbf{k}_4) | \Omega \rangle^{SE}$ are zero at this order. This is a direct consequence of the absence of the interactions Q_s^3 and $Q_\sigma^2 Q_s$ in the third order interaction Hamiltonian (A2). In terms of diagrams this fact is clear. With the interactions (A3) one cannot draw diagrams with one and three external entropy legs, respectively.

In order to find the non-zero four-point functions we need the following set of rules. We draw the allowed diagrams with two of the vertices (A3), where one leg of the first vertex is glued with one leg of the other vertex (entropy legs can only be glued with entropy legs, similarly for adiabatic legs). The resulting four-point function can be constructed as:

- Multiply by $-2(2\pi)^3 \delta^{(3)}(\mathbf{K}) N^4 / (k_1 k_2 k_3 k_4)^{3/2}$, where N is the normalization of the mode functions. Multiply by the coupling constants of the vertices that enter the diagram. The overall minus sign is already present in (A1). The Dirac delta function ensures momentum conservation. The factor $N^4 / (k_1 k_2 k_3 k_4)^{3/2}$ comes from the normalization of the four external legs, described by F . Finally, the factor of two can be understood if one notes that the contribution to the four-point function coming from the first term in the r.h.s. of Eq. (A5) is real and the operator in the second term is just the Hermitian conjugate of the first term. Similarly with the third and fourth terms in the r.h.s. of Eq. (A5).
- To each leg of the vertex with a spatial derivative associate the usual factor $-i\mathbf{k}$.
- The different ways of drawing the same-looking diagram (ignoring the k labels but with the order in the left-to-right of the vertices the same) give a multiplicative symmetry factor.
- The contribution coming from the third (and fourth) term in the r.h.s. of Eq. (A5) is equal to the contribution coming from the first (and second) term but with the sign of k_1 and k_2 (but not k_{12}), that enter the arguments of \mathcal{F}_i functions, changed to minus sign.
- In the diagrams with vertices H_1^{int} or H_3^{int} the form factor is made of \mathcal{F}_1 functions. The definitions of the \mathcal{F}_i functions can be found in Appendix B. In the diagrams with vertices H_2^{int} , H_4^{int} or H_5^{int} the form factor is made of \mathcal{F}_2 functions. In the diagrams where the l.h.s. vertex is either one of H_1^{int} or H_3^{int} and the r.h.s. vertex is either one of H_2^{int} , H_4^{int} or H_5^{int} , the form factor is made of \mathcal{F}_3 functions. In the diagrams where the l.h.s. vertex is either one of H_2^{int} , H_4^{int} or H_5^{int} and the r.h.s. vertex is either one of H_1^{int} or H_3^{int} , the form factor is made of \mathcal{F}_4 functions. The order of the six arguments in \mathcal{F}_i is read from the diagrams too. The first three arguments are read from the l.h.s. vertex and the last three arguments from the r.h.s. vertex. For example, for the diagram made of two H_3^{int} vertices, the first and fourth arguments of \mathcal{F}_2 are the legs with time derivatives. \mathbf{k}_1 in the first vertex and \mathbf{k}_4 in the second vertex.

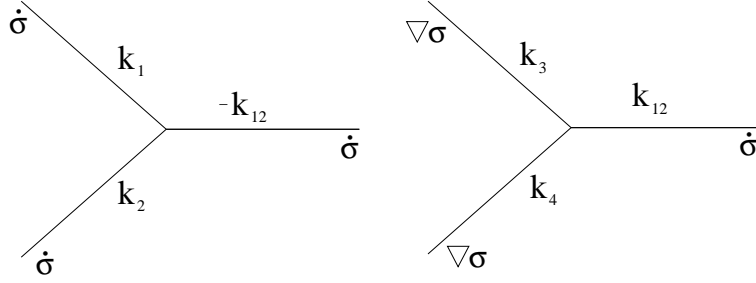


FIG. 7: The two leading order vertices that contribute for the scalar exchange trispectrum in the single field case. Dot over σ denotes that in that leg the interaction is a time derivative. $\nabla\sigma$ means that the interaction is a spatial derivative. There is momentum conservation at the vertices, hence at each vertex the momentum vectors have to sum to zero. Overall momentum conservation implies that $\mathbf{k}_{12} = -\mathbf{k}_{34}$, hence the labels in the r.h.s. diagram.

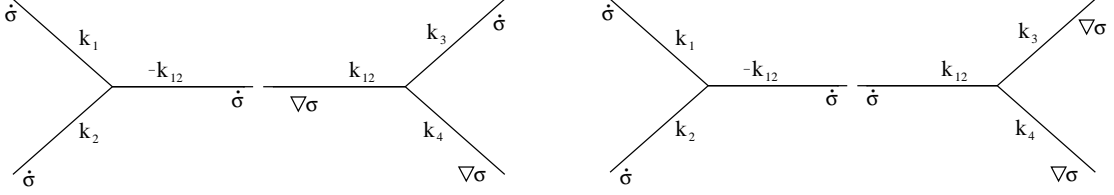


FIG. 8: The two diagrams that contribute to the adiabatic four-point function, where the l.h.s. vertex is H_1^{int} and the r.h.s. vertex is H_2^{int} . The first, on the l.h.s. panel, we glue two legs with a time and a spatial derivative. The second, on the r.h.s. panel, we glue two legs with time derivatives.

- At the end, add twenty three permutations of $\{k_1, k_2, k_3, k_4\}$ to restore the symmetry of the four-point functions under the exchange of the momentum vectors.

Let us consider an explicit example and calculate the contribution for the adiabatic four-point function of a diagram where the l.h.s. vertex is H_1^{int} and the r.h.s. vertex is H_2^{int} . These vertices are schematically depicted in Fig. 7 and they are the same ones as in the single field case.

There are two distinct diagrams that one can draw, as can be seen in Fig. 8, hence there will be two terms. For the diagram on the l.h.s. of Fig. 8 we get a symmetry factor six. This is because there are three ways we can glue the $\nabla\sigma$ leg to the $\dot{\sigma}$ leg and there are two $\nabla\sigma$ legs. For the diagram on the r.h.s. of Fig. 8 we get a symmetry factor three. This is because there are three ways of gluing the $\dot{\sigma}$ leg of the H_2^{int} vertex with one of the $\dot{\sigma}$ legs of the H_1^{int} vertex. In both diagrams, we have two spatial derivatives so we get a factor $(-i)^2$. These diagrams will be proportional to \mathcal{F}_3 .

Finally, the diagram on the l.h.s. gives

$$\begin{aligned}
& \langle \Omega | Q_\sigma(0, \mathbf{k}_1) Q_\sigma(0, \mathbf{k}_2) Q_\sigma(0, \mathbf{k}_3) Q_\sigma(0, \mathbf{k}_4) | \Omega \rangle^{SE} \\
& \supset (-i)^2 6 (2\pi)^3 \delta(\mathbf{K}) \frac{-2N^4 g_1 g_2}{(k_1 k_2 k_3 k_4)^{\frac{3}{2}}} (\mathbf{k}_{12} \cdot \mathbf{k}_4) (\mathcal{F}_3(k_1, k_2, -k_{12}, k_3, k_4, k_{12}) - \mathcal{F}_3(-k_1, -k_2, -k_{12}, k_3, k_4, k_{12})) \\
& + 23 \text{ permutations of } \{k_1, k_2, k_3, k_4\}, \tag{A6}
\end{aligned}$$

and the diagram in the r.h.s. gives

$$\begin{aligned}
& \langle \Omega | Q_\sigma(0, \mathbf{k}_1) Q_\sigma(0, \mathbf{k}_2) Q_\sigma(0, \mathbf{k}_3) Q_\sigma(0, \mathbf{k}_4) | \Omega \rangle^{SE} \\
& \supset (-i)^2 3 (2\pi)^3 \delta(\mathbf{K}) \frac{-2N^4 g_1 g_2}{(k_1 k_2 k_3 k_4)^{\frac{3}{2}}} (\mathbf{k}_3 \cdot \mathbf{k}_4) (\mathcal{F}_3(k_1, k_2, -k_{12}, k_{12}, k_3, k_4) - \mathcal{F}_3(-k_1, -k_2, -k_{12}, k_{12}, k_3, k_4)) \\
& + 23 \text{ permutations of } \{k_1, k_2, k_3, k_4\} \tag{A7}
\end{aligned}$$

Now, let us consider another example and calculate the contribution for the mixed four-point function of a diagram where the l.h.s. vertex is H_4^{int} and the r.h.s. vertex is H_5^{int} . These diagrams involves vertices that contain entropy legs, they are schematically depicted in Fig. 9.

Because the entropy and the adiabatic mode functions are the same, if one substitutes s with σ in the vertices of Fig. 9 we get the vertices of Fig. 7. Because the \mathcal{F}_i functions only depend on the mode functions, that are the same

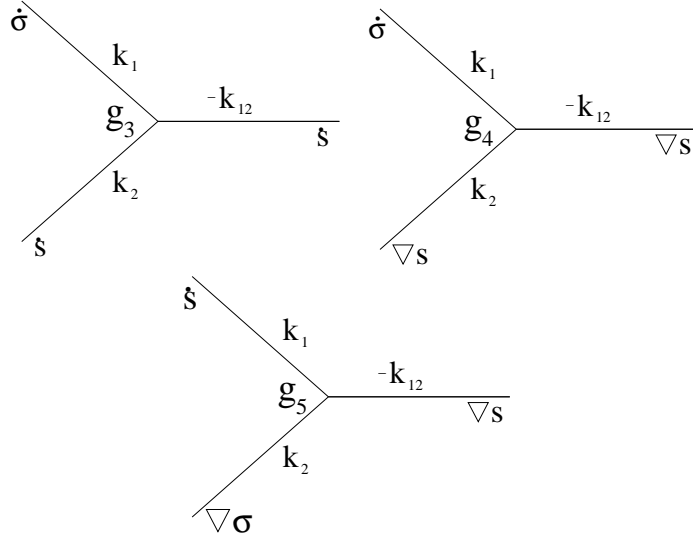


FIG. 9: The leading order vertices containing entropy modes that contribute for the scalar exchange trispectrum in the multi-field case. g_i denotes the coupling constants. As before, the dot over s denotes that in that leg the interaction is a time derivative. ∇s means that the interaction is a spatial derivative. A label s in the leg means that it is a entropy mode. σ denotes an adiabatic leg.

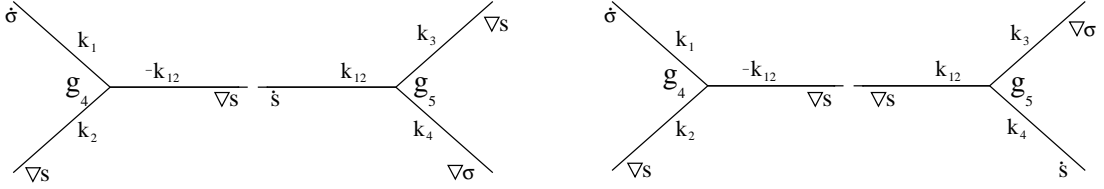


FIG. 10: The two diagrams that contribute to the mixed four-point function, where the l.h.s. vertex is H_4^{int} and the r.h.s. vertex is H_5^{int} .

for the entropy and the adiabatic modes we don't need to define other \mathcal{F}_i functions, and the single field ones are enough.

There are two diagrams that contribute in this example, as can be seen in Fig. 10, hence there will be two terms. In both diagrams, we have four spatial derivatives, this gives a factor of $(-i)^4$. The diagram on the l.h.s. of the figure has a symmetry factor two, because there are two ways of gluing the \dot{s} leg of the r.h.s. vertex with one of the two ∇s legs of the l.h.s. vertex. Similarly, the symmetry factor of the r.h.s. diagram is also two.

The l.h.s. diagram contributes with

$$\begin{aligned} & \langle \Omega | Q_\sigma(0, \mathbf{k}_1) Q_\sigma(0, \mathbf{k}_2) Q_s(0, \mathbf{k}_3) \overline{Q_s}(0, \mathbf{k}_4) | \Omega \rangle^{SE} + 5 \text{ perms.} \\ & \supset (-i)^4 2 (2\pi)^3 \delta(\mathbf{K}) \frac{-2N^4 g_4 g_5}{(k_1 k_2 k_3 k_4)^{\frac{3}{2}}} (\mathbf{k}_2 \cdot (-\mathbf{k}_{12})) (\mathbf{k}_3 \cdot \mathbf{k}_4) (\mathcal{F}_2(k_1, k_2, -k_{12}, k_{12}, k_3, k_4) - \mathcal{F}_2(-k_1, -k_2, -k_{12}, k_{12}, k_3, k_4)) \\ & \quad + 23 \text{ permutations of } \{k_1, k_2, k_3, k_4\}, \end{aligned} \quad (\text{A8})$$

and the diagram in the r.h.s. gives

$$\begin{aligned} & \langle \Omega | Q_\sigma(0, \mathbf{k}_1) Q_\sigma(0, \mathbf{k}_2) Q_s(0, \mathbf{k}_3) \overline{Q_s}(0, \mathbf{k}_4) | \Omega \rangle^{SE} + 5 \text{ perms.} \\ & \supset (-i)^4 2 (2\pi)^3 \delta(\mathbf{K}) \frac{-2N^4 g_4 g_5}{(k_1 k_2 k_3 k_4)^{\frac{3}{2}}} (\mathbf{k}_2 \cdot (-\mathbf{k}_{12})) (\mathbf{k}_{12} \cdot \mathbf{k}_4) (\mathcal{F}_2(k_1, k_2, -k_{12}, k_4, k_3, k_{12}) - \mathcal{F}_2(-k_1, -k_2, -k_{12}, k_4, k_3, k_{12})) \\ & \quad + 23 \text{ permutations of } \{k_1, k_2, k_3, k_4\}, \end{aligned} \quad (\text{A9})$$

where 5 perms. denotes the following permutations of the displayed term $[1 \leftrightarrow 3]$, $[1 \leftrightarrow 4]$, $[2 \leftrightarrow 3]$, $[2 \leftrightarrow 4]$ and $[1 \leftrightarrow 3, 2 \leftrightarrow 4]$.

APPENDIX B: DEFINITIONS OF THE \mathcal{F}_i FUNCTIONS

In this Appendix, we present the definitions and the analytical expressions of the four \mathcal{F}_i functions (with $i = 1, \dots, 4$) that appear in the main text.

Because there are only four different types of double time integrals over the mode functions, we define four \mathcal{F}_i functions (with $i = 1, \dots, 4$). Their explicit expressions are

$$\begin{aligned} \mathcal{F}_1(k_1, k_2, k_3, k_4, k_5, k_6) &= \int_{-\infty}^0 d\eta a(\eta) \int_{-\infty}^{\eta} d\tilde{\eta} a(\tilde{\eta}) U^{*'}(\eta, k_1) U^{*'}(\eta, k_2) U^{*'}(\eta, k_3) U^{*'}(\tilde{\eta}, k_4) U^{*'}(\tilde{\eta}, k_5) U^{*'}(\tilde{\eta}, k_6) \\ &= -4 \frac{N^6 c_s^6}{H^2} |k_1 \dots k_6|^{\frac{1}{2}} \frac{1}{\mathcal{A}^3 \mathcal{C}^3} \left(1 + 3 \frac{\mathcal{A}}{\mathcal{C}} + 6 \frac{\mathcal{A}^2}{\mathcal{C}^2} \right), \end{aligned} \quad (\text{B1})$$

where N is the normalisation of the mode functions given by $N = H/\sqrt{2c_s}$, \mathcal{A} is defined by the sum of the last three arguments of the \mathcal{F}_i functions as $\mathcal{A} = k_4 + k_5 + k_6$ and \mathcal{C} is defined by the sum of all the arguments as $\mathcal{C} = k_1 + k_2 + k_3 + k_4 + k_5 + k_6$. The remaining functions are

$$\begin{aligned} \mathcal{F}_2(k_1, k_2, k_3, k_4, k_5, k_6) &= \int_{-\infty}^0 d\eta a(\eta) \int_{-\infty}^{\eta} d\tilde{\eta} a(\tilde{\eta}) U^{*'}(\eta, k_1) U^*(\eta, k_2) U^*(\eta, k_3) U^{*'}(\tilde{\eta}, k_4) U^*(\tilde{\eta}, k_5) U^*(\tilde{\eta}, k_6) \\ &= -\frac{N^6 c_s^2}{H^2} \frac{|k_1 k_4|^{\frac{1}{2}}}{|k_2 k_3 k_5 k_6|^{\frac{3}{2}}} \frac{1}{\mathcal{A} \mathcal{C}} \left[1 + \frac{k_5 + k_6}{\mathcal{A}} + 2 \frac{k_5 k_6}{\mathcal{A}^2} \right. \\ &\quad \left. + \frac{1}{\mathcal{C}} \left(k_2 + k_3 + k_5 + k_6 + \frac{1}{\mathcal{A}} \left((k_2 + k_3)(k_5 + k_6) + 2k_5 k_6 \right) + 2 \frac{k_5 k_6 (k_2 + k_3)}{\mathcal{A}^2} \right) \right. \\ &\quad \left. + \frac{2}{\mathcal{C}^2} \left(k_5 k_6 + (k_2 + k_3)(k_5 + k_6) + k_2 k_3 \right. \right. \\ &\quad \left. \left. + \frac{1}{\mathcal{A}} (k_2 k_3 (k_5 + k_6) + 2k_5 k_6 (k_2 + k_3)) + 2 \frac{k_2 k_3 k_5 k_6}{\mathcal{A}^2} \right) \right. \\ &\quad \left. + \frac{6}{\mathcal{C}^3} \left(k_2 k_3 (k_5 + k_6) + k_5 k_6 (k_2 + k_3) + 2 \frac{k_2 k_3 k_5 k_6}{\mathcal{A}} \right) + 24 \frac{k_2 k_3 k_5 k_6}{\mathcal{C}^4} \right], \end{aligned} \quad (\text{B2})$$

$$\begin{aligned} \mathcal{F}_3(k_1, k_2, k_3, k_4, k_5, k_6) &= \int_{-\infty}^0 d\eta a(\eta) \int_{-\infty}^{\eta} d\tilde{\eta} a(\tilde{\eta}) U^{*'}(\eta, k_1) U^{*'}(\eta, k_2) U^{*'}(\eta, k_3) U^{*'}(\tilde{\eta}, k_4) U^*(\tilde{\eta}, k_5) U^*(\tilde{\eta}, k_6) \\ &= 2 \frac{N^6 c_s^4}{H^2} \frac{|k_1 k_2 k_3 k_4|^{\frac{1}{2}}}{|k_5 k_6|^{\frac{3}{2}}} \frac{1}{\mathcal{A} \mathcal{C}^3} \left[1 + \frac{k_5 + k_6}{\mathcal{A}} + 2 \frac{k_5 k_6}{\mathcal{A}^2} + \frac{3}{\mathcal{C}} \left(k_5 + k_6 + 2 \frac{k_5 k_6}{\mathcal{A}} \right) + 12 \frac{k_5 k_6}{\mathcal{C}^2} \right], \end{aligned} \quad (\text{B3})$$

$$\begin{aligned} \mathcal{F}_4(k_1, k_2, k_3, k_4, k_5, k_6) &= \int_{-\infty}^0 d\eta a(\eta) \int_{-\infty}^{\eta} d\tilde{\eta} a(\tilde{\eta}) U^{*'}(\eta, k_1) U^*(\eta, k_2) U^*(\eta, k_3) U^{*'}(\tilde{\eta}, k_4) U^{*'}(\tilde{\eta}, k_5) U^{*'}(\tilde{\eta}, k_6) \\ &= 2 \frac{N^6 c_s^4}{H^2} \frac{|k_1 k_4 k_5 k_6|^{\frac{1}{2}}}{|k_2 k_3|^{\frac{3}{2}}} \frac{1}{\mathcal{A}^3 \mathcal{C}} \left[1 + \frac{\mathcal{A}}{\mathcal{C}} + \frac{\mathcal{A}^2}{\mathcal{C}^2} + \frac{k_2 + k_3}{\mathcal{C}} + 2 \frac{\mathcal{A} (k_2 + k_3) + k_2 k_3}{\mathcal{C}^2} \right. \\ &\quad \left. + 3 \frac{\mathcal{A}}{\mathcal{C}^3} (\mathcal{A} (k_2 + k_3) + 2k_2 k_3) + 12k_2 k_3 \frac{\mathcal{A}^2}{\mathcal{C}^4} \right], \end{aligned} \quad (\text{B4})$$

where the function $U(\eta, k)$ is a modified mode function given by

$$U(\eta, k) = N \frac{1}{|k|^{\frac{3}{2}}} (1 + ikc_s \eta) e^{-ikc_s \eta}. \quad (\text{B5})$$

If the sign of the argument k of U is positive then U is equal to the mode function, if the sign is negative then U equals the complex conjugate of the mode function.

APPENDIX C: THE SCALAR EXCHANGE TRISPECTRUM IN THE EQUILATERAL LIMIT

In this Appendix, we present the scalar exchange trispectrum of the primordial curvature perturbation \mathcal{R} in the equilateral configuration. These analytical expressions can be derived from the general expression for the scalar exchange trispectrum, Eq. (43). We will use these simpler equations to study the shape dependence of the trispectrum and to calculate the non-linearity parameter τ_{NL} in subsection V B.

At leading order in the small sound speed and in the slow-roll expansion, the scalar exchange trispectrum is

$$\begin{aligned} \langle \Omega | \mathcal{R}(0, \mathbf{k}_1) \mathcal{R}(0, \mathbf{k}_2) \mathcal{R}(0, \mathbf{k}_3) \mathcal{R}(0, \mathbf{k}_4) | \Omega \rangle^{SE} &= \langle \Omega | \mathcal{R}(0, \mathbf{k}_1) \mathcal{R}(0, \mathbf{k}_2) \mathcal{R}(0, \mathbf{k}_3) \mathcal{R}(0, \mathbf{k}_4) | \Omega \rangle^{SE}_{4\sigma} \\ &+ \langle \Omega | \mathcal{R}(0, \mathbf{k}_1) \mathcal{R}(0, \mathbf{k}_2) \mathcal{R}(0, \mathbf{k}_3) \mathcal{R}(0, \mathbf{k}_4) | \Omega \rangle^{SE}_{\sigma\sigma ss} \\ &+ \langle \Omega | \mathcal{R}(0, \mathcal{R}k_1) \mathcal{R}(0, \mathbf{k}_2) \mathcal{R}(0, \mathbf{k}_3) \mathcal{R}(0, \mathbf{k}_4) | \Omega \rangle^{SE}_{4s}, \end{aligned} \quad (C1)$$

where the three different contributions come from the terms in Eq. (43) that are coming from the purely adiabatic, mixed and purely entropy components.

Explicitly, they are given by

$$\langle \Omega | \mathcal{R}(0, \mathbf{k}_1) \mathcal{R}(0, \mathbf{k}_2) \mathcal{R}(0, \mathbf{k}_3) \mathcal{R}(0, \mathbf{k}_4) | \Omega \rangle^{SE}_{4\sigma} = (2\pi)^3 \delta^{(3)}(\mathbf{K}) \frac{1}{c_s^4} \frac{1}{(1 + T_{\mathcal{RS}}^2)^3} \mathcal{D}_1(k_{12}/k) \tilde{\mathcal{P}}_{\mathcal{R}*}^2(k) \tilde{\mathcal{P}}_{\mathcal{R}*}(k_{12}) + 2 \text{ perms}, \quad (C2)$$

$$\langle \Omega | \mathcal{R}(0, \mathbf{k}_1) \mathcal{R}(0, \mathbf{k}_2) \mathcal{R}(0, \mathbf{k}_3) \mathcal{R}(0, \mathbf{k}_4) | \Omega \rangle^{SE}_{\sigma\sigma ss} = (2\pi)^3 \delta^{(3)}(\mathbf{K}) \frac{T_{\mathcal{RS}}^2}{(1 + T_{\mathcal{RS}}^2)^3} \frac{1}{c_s^4} \mathcal{D}_2(k_{12}/k) \tilde{\mathcal{P}}_{\mathcal{R}*}^2(k) \tilde{\mathcal{P}}_{\mathcal{R}*}(k_{12}) + 2 \text{ perms}, \quad (C3)$$

$$\langle \Omega | \mathcal{R}(0, \mathbf{k}_1) \mathcal{R}(0, \mathbf{k}_2) \mathcal{R}(0, \mathbf{k}_3) \mathcal{R}(0, \mathbf{k}_4) | \Omega \rangle^{SE}_{4s} = (2\pi)^3 \delta^{(3)}(\mathbf{K}) \frac{T_{\mathcal{RS}}^4}{(1 + T_{\mathcal{RS}}^2)^3} \frac{1}{c_s^4} \mathcal{D}_3(k_{12}/k) \tilde{\mathcal{P}}_{\mathcal{R}*}^2(k) \tilde{\mathcal{P}}_{\mathcal{R}*}(k_{12}) + 2 \text{ perms}, \quad (C4)$$

where we have defined three $\mathcal{D}_i(x)$ functions, with $i = 1, 2, 3$, as

$$\begin{aligned} \mathcal{D}_1(x) &= \frac{x^4(61952 + 48384x - 10240x^2 - 20832x^3 - 5184x^4 + 1412x^5 + 824x^6 + 103x^7)}{2^9(x+2)^4}, \\ \mathcal{D}_2(x) &= \frac{x^4(31232 + 23744x - 6272x^2 - 10496x^3 - 1248x^4 + 1904x^5 + 824x^6 + 103x^7)}{2^8(x+2)^4}, \\ \mathcal{D}_3(x) &= \frac{x^4(512 - 896x - 2304x^2 - 160x^3 + 2688x^4 + 2396x^5 + 824x^6 + 103x^7)}{2^9(x+2)^4}, \end{aligned} \quad (C5)$$

where $k_{12} = k\sqrt{2(1 + \cos\theta_3)}$, $k_{13} = k\sqrt{2(1 + \cos\theta_2)}$ and $k_{14} = k\sqrt{2(1 + \cos\theta_1)}$. k denotes the common amplitude of all four momentum vectors \mathbf{k}_j , with $j = 1, \dots, 4$ and the rescaled power spectrum is $\tilde{\mathcal{P}}_{\mathcal{R}*}(k) = H^2/(4\epsilon c_s k^3)$ that should be evaluated at sound horizon crossing.

It is worth mentioning that from Eqs. (37) and (44), the following relation holds,

$$\mathcal{D}_2 = \mathcal{D}_1 + \mathcal{D}_3. \quad (C6)$$

[1] <http://map.gsfc.nasa.gov/>.

[2] A. P. S. Yadav and B. D. Wandelt, Phys. Rev. Lett. **100**, 181301 (2008), 0712.1148.

[3] WMAP, E. Komatsu *et al.*, Astrophys. J. Suppl. **180**, 330 (2009), 0803.0547.

[4] K. M. Smith, L. Senatore and M. Zaldarriaga, JCAP **0909** (2009) 006 [arXiv:0901.2572 [astro-ph]].

[5] <http://www.rssd.esa.int/index.php?project=Planck>

[6] J. M. Maldacena, JHEP **0305** (2003) 013 [arXiv:astro-ph/0210603].

[7] A. D. Linde and V. F. Mukhanov, Phys. Rev. **D56**, R535 (1997), astro-ph/9610219.

[8] N. Bartolo, S. Matarrese, and A. Riotto, Phys. Rev. **D65**, 103505 (2002), hep-ph/0112261.

- [9] F. Bernardeau and J.-P. Uzan, Phys. Rev. **D66**, 103506 (2002), hep-ph/0207295.
- [10] F. Bernardeau and J.-P. Uzan, Phys. Rev. **D67**, 121301 (2003), astro-ph/0209330.
- [11] G. Dvali, A. Gruzinov, and M. Zaldarriaga, Phys. Rev. **D69**, 023505 (2004), astro-ph/0303591.
- [12] P. Creminelli, JCAP **0310**, 003 (2003), astro-ph/0306122.
- [13] M. Alishahiha, E. Silverstein and D. Tong, Phys. Rev. D **70** (2004) 123505 [arXiv:hep-th/0404084].
- [14] A. Gruzinov, Phys. Rev. **D71**, 027301 (2005), astro-ph/0406129.
- [15] N. Bartolo, E. Komatsu, S. Matarrese and A. Riotto, Phys. Rept. **402**, 103 (2004) [arXiv:astro-ph/0406398].
- [16] K. Enqvist, A. Jokinen, A. Mazumdar, T. Multamaki, and A. Vaihkonen, Phys. Rev. Lett. **94**, 161301 (2005), astro-ph/0411394.
- [17] D. Seery and J. E. Lidsey, JCAP **0506** (2005) 003 [arXiv:astro-ph/0503692].
- [18] D. Seery and J. E. Lidsey, JCAP **0509** (2005) 011 [arXiv:astro-ph/0506056].
- [19] A. Jokinen and A. Mazumdar, JCAP **0604**, 003 (2006), astro-ph/0512368.
- [20] D. H. Lyth, JCAP **0511**, 006 (2005), astro-ph/0510443.
- [21] M. P. Salem, Phys. Rev. **D72**, 123516 (2005), astro-ph/0511146.
- [22] D. Seery and J. E. Lidsey, JCAP **0701**, 008 (2007), astro-ph/0611034.
- [23] M. Sasaki, J. Valiviita, and D. Wands, Phys. Rev. **D74**, 103003 (2006), astro-ph/0607627.
- [24] K. A. Malik and D. H. Lyth, JCAP **0609**, 008 (2006), astro-ph/0604387.
- [25] N. Barnaby and J. M. Cline, Phys. Rev. **D73**, 106012 (2006), astro-ph/0601481.
- [26] L. Alabidi and D. Lyth, JCAP **0608**, 006 (2006), astro-ph/0604569.
- [27] X. Chen, M. x. Huang, S. Kachru and G. Shiu, JCAP **0701** (2007) 002 [arXiv:hep-th/0605045].
- [28] X. Chen, M. x. Huang and G. Shiu, Phys. Rev. D **74** (2006) 121301 [arXiv:hep-th/0610235].
- [29] X. Chen, R. Easther, and E. A. Lim, JCAP **0706**, 023 (2007), astro-ph/0611645.
- [30] L. Alabidi, JCAP **0610**, 015 (2006), astro-ph/0604611.
- [31] D. Seery, J. E. Lidsey and M. S. Sloth, JCAP **0701**, 027 (2007) [arXiv:astro-ph/0610210].
- [32] C. T. Byrnes, M. Sasaki, and D. Wands, Phys. Rev. **D74**, 123519 (2006), astro-ph/0611075.
- [33] T. Suyama and M. Yamaguchi, Phys. Rev. **D77**, 023505 (2008), 0709.2545.
- [34] F. Arroja and K. Koyama, Phys. Rev. D **77**, 083517 (2008) [arXiv:0802.1167 [hep-th]].
- [35] F. Arroja, S. Mizuno and K. Koyama, JCAP **0808**, 015 (2008) [arXiv:0806.0619 [astro-ph]].
- [36] D. Langlois, S. Renaux-Petel, D. A. Steer and T. Tanaka, Phys. Rev. Lett. **101**, 061301 (2008) [arXiv:0804.3139 [hep-th]].
- [37] D. Langlois, S. Renaux-Petel, D. A. Steer and T. Tanaka, Phys. Rev. D **78**, 063523 (2008) [arXiv:0806.0336 [hep-th]].
- [38] D. Seery, M. S. Sloth and F. Vernizzi, JCAP **0903**, 018 (2009) [arXiv:0811.3934 [astro-ph]].
- [39] M. Sasaki, Prog. Theor. Phys. **120**, 159 (2008), 0805.0974.
- [40] C. T. Byrnes, K.-Y. Choi, and L. M. H. Hall, JCAP **0810**, 008 (2008), 0807.1101.
- [41] C. T. Byrnes, K.-Y. Choi, and L. M. H. Hall, JCAP **0902**, 017 (2009), 0812.0807.
- [42] B. Dutta, L. Leblond, and J. Kumar, Phys. Rev. **D78**, 083522 (2008), 0805.1229.
- [43] A. Naruko and M. Sasaki, Prog. Theor. Phys. **121**, 193 (2009), 0807.0180.
- [44] T. Suyama and F. Takahashi, JCAP **0809**, 007 (2008), 0804.0425.
- [45] X. Gao, JCAP **0806**, 029 (2008) [arXiv:0804.1055 [astro-ph]].
- [46] H. R. S. Cogollo, Y. Rodriguez, and C. A. Valenzuela-Toledo, JCAP **0808**, 029 (2008), 0806.1546.
- [47] Y. Rodriguez and C. A. Valenzuela-Toledo, (2008), 0811.4092.
- [48] K. Ichikawa, T. Suyama, T. Takahashi, and M. Yamaguchi, Phys. Rev. **D78**, 023513 (2008), 0802.4138.
- [49] C. T. Byrnes, JCAP **0901**, 011 (2009), 0810.3913.
- [50] S. Li, Y.-F. Cai, and Y.-S. Piao, Phys. Lett. **B671**, 423 (2009), 0806.2363.
- [51] D. Langlois, F. Vernizzi, and D. Wands, JCAP **0812**, 004 (2008), 0809.4646.
- [52] C. Hikage, K. Koyama, T. Matsubara, T. Takahashi, and M. Yamaguchi, (2008), 0812.3500.
- [53] M. Kawasaki, K. Nakayama, T. Sekiguchi, T. Suyama, and F. Takahashi, JCAP **0811**, 019 (2008), 0808.0009.
- [54] Q. G. Huang, JCAP **0811** (2008) 005 [arXiv:0808.1793 [hep-th]].
- [55] X. Gao and B. Hu, JCAP **0908**, 012 (2009) [arXiv:0903.1920 [astro-ph.CO]].
- [56] Y. F. Cai and H. Y. Xia, Phys. Lett. B **677** (2009) 226 [arXiv:0904.0062 [hep-th]].
- [57] D. Langlois, S. Renaux-Petel and D. A. Steer, JCAP **0904**, 021 (2009) [arXiv:0902.2941 [hep-th]].
- [58] X. Gao, (2009), 0904.4187.
- [59] Q. G. Huang, JCAP **0905**, 005 (2009) [arXiv:0903.1542 [hep-th]].
- [60] Q. G. Huang, JCAP **0906**, 035 (2009) [arXiv:0904.2649 [hep-th]].
- [61] J. Khoury and F. Piazza, JCAP **0907**, 026 (2009) [arXiv:0811.3633 [hep-th]].
- [62] F. Arroja, S. Mizuno, K. Koyama and T. Tanaka, Phys. Rev. D **80**, 043527 (2009) [arXiv:0905.3641 [hep-th]].
- [63] X. Chen, B. Hu, M. x. Huang, G. Shiu and Y. Wang, JCAP **0908**, 008 (2009) [arXiv:0905.3494 [astro-ph.CO]].
- [64] S. Mizuno, F. Arroja, K. Koyama and T. Tanaka, Phys. Rev. D **80**, 023530 (2009) [arXiv:0905.4557 [hep-th]].
- [65] C. T. Byrnes and G. Tasinato, JCAP **0908**, 016 (2009) [arXiv:0906.0767 [astro-ph.CO]].
- [66] X. Gao, M. Li and C. Lin, arXiv:0906.1345 [astro-ph.CO].
- [67] C. Armendariz-Picon, T. Damour and V. F. Mukhanov, Phys. Lett. B **458** (1999) 209 [arXiv:hep-th/9904075].
- [68] J. Garriga and V. F. Mukhanov, Phys. Lett. B **458** (1999) 219 [arXiv:hep-th/9904176].
- [69] E. Silverstein and D. Tong, Phys. Rev. D **70** (2004) 103505 [arXiv:hep-th/0310221].
- [70] X. Chen, Phys. Rev. D **71** (2005) 063506 [arXiv:hep-th/0408084].
- [71] X. Chen, JHEP **0508** (2005) 045 [arXiv:hep-th/0501184].

- [72] X. Chen, Phys. Rev. D **72** (2005) 123518 [arXiv:astro-ph/0507053].
- [73] S. Kecskesti, J. Maiden, G. Shiu and B. Underwood, JHEP **0609**, 076 (2006) [arXiv:hep-th/0605189].
- [74] J. E. Lidsey and D. Seery, Phys. Rev. **D75**, 043505 (2007), astro-ph/0610398.
- [75] D. Baumann and L. McAllister, Phys. Rev. D **75**, 123508 (2007) [arXiv:hep-th/0610285].
- [76] R. Bean, S. E. Shandera, S. H. Henry Tye and J. Xu, JCAP **0705**, 004 (2007) [arXiv:hep-th/0702107].
- [77] J. E. Lidsey and I. Huston, JCAP **0707**, 002 (2007) [arXiv:0705.0240 [hep-th]].
- [78] H. V. Peiris, D. Baumann, B. Friedman, and A. Cooray, Phys. Rev. **D76**, 103517 (2007), 0706.1240.
- [79] T. Kobayashi, S. Mukohyama and S. Kinoshita, JCAP **0801**, 028 (2008) [arXiv:0708.4285 [hep-th]].
- [80] F. Gmeiner and C. D. White, JCAP **0802** (2008) 012 [arXiv:0710.2009 [hep-th]].
- [81] L. Lorenz, J. Martin, and C. Ringeval, JCAP **0804**, 001 (2008), 0709.3758.
- [82] R. Bean, X. Chen, H. Peiris and J. Xu, Phys. Rev. D **77**, 023527 (2008) [arXiv:0710.1812 [hep-th]].
- [83] S. Bird, H. V. Peiris and D. Baumann, Phys. Rev. D **80**, 023534 (2009) [arXiv:0905.2412 [hep-th]].
- [84] D. A. Easson, R. Gregory, D. F. Mota, G. Tasinato and I. Zavala, JCAP **0802** (2008) 010 [arXiv:0709.2666 [hep-th]].
- [85] A. A. Starobinsky and J. Yokoyama, arXiv:gr-qc/9502002.
- [86] M. x. Huang, G. Shiu and B. Underwood, Phys. Rev. D **77** (2008) 023511 [arXiv:0709.3299 [hep-th]].
- [87] D. Langlois and S. Renaux-Petel, JCAP **0804** (2008) 017 [arXiv:0801.1085 [hep-th]].
- [88] S. Renaux-Petel and G. Tasinato, JCAP **0901** (2009) 012 [arXiv:0810.2405 [hep-th]].
- [89] L. Boubekeur and D. H. Lyth, Phys. Rev. D **73**, 021301 (2006) [arXiv:astro-ph/0504046].
- [90] L. Alabidi and D. H. Lyth, JCAP **0605**, 016 (2006) [arXiv:astro-ph/0510441].
- [91] N. Kogo and E. Komatsu, Phys. Rev. D **73**, 083007 (2006) [arXiv:astro-ph/0602099].
- [92] D. Babich, P. Creminelli and M. Zaldarriaga, JCAP **0408**, 009 (2004) [arXiv:astro-ph/0405356].
- [93] W. Hu, Phys. Rev. D **64**, 083005 (2001) [arXiv:astro-ph/0105117].
- [94] T. Okamoto and W. Hu, Phys. Rev. D **66**, 063008 (2002) [arXiv:astro-ph/0206155].
- [95] P. Creminelli, L. Senatore and M. Zaldarriaga, JCAP **0703**, 019 (2007) [arXiv:astro-ph/0606001].
- [96] R. G. Leigh, Mod. Phys. Lett. A **4**, 2767 (1989).
- [97] C. Gordon, D. Wands, B. A. Bassett and R. Maartens, Phys. Rev. D **63** (2000) 023506 [arXiv:astro-ph/0009131].
- [98] R. Arnowitt, S. Deser and C. W. Misner, Phys. Rev. **117** (1960) 1595.
- [99] S. Weinberg, Phys. Rev. D **72** (2005) 043514 [arXiv:hep-th/0506236].
- [100] D. Wands, N. Bartolo, S. Matarrese and A. Riotto, Phys. Rev. D **66** (2002) 043520 [arXiv:astro-ph/0205253].
- [101] P. Creminelli and M. Zaldarriaga, JCAP **0410**, 006 (2004), astro-ph/0407059.
- [102] C. Cheung, A. L. Fitzpatrick, J. Kaplan, and L. Senatore, JCAP **0802**, 021 (2008), 0709.0295.
- [103] H-Y. Chen, J-O. Gong, K. Koyama and G. Tasinato, in preparation.
- [104] S. Renaux-Petel, arXiv:0907.2476 [hep-th].